



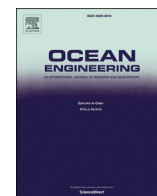
## CFD based form factor determination method

Downloaded from: <https://research.chalmers.se>, 2023-05-06 00:13 UTC

Citation for the original published paper (version of record):

Korkmaz, K., Werner, S., Sakamoto, N. et al (2021). CFD based form factor determination method. Ocean Engineering, 220. <http://dx.doi.org/10.1016/j.oceaneng.2020.108451>

N.B. When citing this work, cite the original published paper.



## CFD based form factor determination method

Kadir Burak Korkmaz<sup>a,b,\*</sup>, Sofia Werner<sup>a</sup>, Nobuaki Sakamoto<sup>c</sup>, Patrick Queutey<sup>d</sup>,  
Ganbo Deng<sup>d</sup>, Gao Yuling<sup>e</sup>, Dong Guoxiang<sup>e</sup>, Kevin Maki<sup>f</sup>, Haixuan Ye<sup>f</sup>, Ayhan Akinturk<sup>g</sup>,  
Tanvir Sayeed<sup>g</sup>, Takanori Hino<sup>h</sup>, Feng Zhao<sup>i</sup>, Tahsin Tezdogan<sup>j</sup>, Yigit Kemal Demirel<sup>j</sup>,  
Rickard Bensow<sup>b</sup>

<sup>a</sup> SSPA Sweden AB, Chalmers Tvärgata 10, Box 24001, Se-400 22, Göteborg, Sweden

<sup>b</sup> Chalmers University of Technology, Sweden

<sup>c</sup> National Maritime Research Institute (NMRI), Japan

<sup>d</sup> LHEEA, CNRS Ecole Centrale de Nantes, France

<sup>e</sup> Shanghai Ship and Shipping Research Institute (SSSRI), China

<sup>f</sup> CSHL University of Michigan, USA

<sup>g</sup> Ocean, Coastal and River Engineering (OCRE), NRC, Canada

<sup>h</sup> Yokohama National University, Japan

<sup>i</sup> China Ship Scientific Research Centre (CSSRC), China

<sup>j</sup> University of Strathclyde, United Kingdom

## ARTICLE INFO

## Keywords:

Ship resistance

Form factor

CFD

Scale effects

Combined CFD/EFD Methods

Experimental uncertainty analysis

## ABSTRACT

The 1978 ITTC Power Prediction method is used to predict the propulsive power of ships through towing tank testing. The form factor approach and its determination in this method have been questioned. This paper investigates the possibility to improve the power predictions by introducing Combined CFD/EFD Method where the experimental determination of form factor is replaced by double body RANS computations applied for open cases KVLCC2 and KCS, including first-time published towing tank tests of KVLCC2 at ballast condition including an experimental uncertainty analysis specifically derived for the form factor. Computations from nine organisations and seven CFD codes are compared to the experiments. The form factor predictions for both hulls in design loading condition compared well with the experimental results in general. For the KVLCC2 ballast condition, majority of the form factors were under-predicted while staying within the experimental uncertainty. Speed dependency is observed with the application of ITTC57 line but it is reduced with the Katsui line and nearly eliminated by numerical friction lines. Comparison of the full-scale viscous resistance predictions obtained by the extrapolations from model scale and direct full-scale computations show that the Combined CFD/EFD Method show significantly less scatter and may thus be a preferred approach.

## 1. Introduction

Performance prediction of a ship is one of the most important tasks during the design phase. As a ship design progresses from beginning to end, the required confidence interval for the prediction method increases. According to the majority of commercial tendencies presented by shipyards and ship owners, towing tank tests are still considered as the last step of the performance prediction. Additionally, legal authorities consider towing tank testing as a mandatory step in their evaluations such as EEDI calculations as enforced by IMO (2011) where the applicable ships must go through the pre-verification by model testing

during the design phase of a new ship.

Towing tank testing has remained as the only practice for more than a century with high accuracy to predict the performance of a ship in deep and calm water since William Froude introduced the extrapolation procedures in the 1870s. The foundation of the International Towing Tank Committee (ITTC) in 1933, lead to improved and standardized procedures in nearly all aspects of performance prediction. An important step towards a common prediction method was taken in 1973 when computer programs with different assumptions and extrapolation methods were created by SSPA as requested by the ITTC (Lindgren and Dyne, 1980). Ten institutions known to have access to sea trials for

\* Corresponding author. SSPA Sweden AB, Sweden.

E-mail address: [burak.korkmaz@sspa.se](mailto:burak.korkmaz@sspa.se) (K.B. Korkmaz).

<https://doi.org/10.1016/j.oceaneng.2020.108451>

Received 16 September 2020; Received in revised form 27 November 2020; Accepted 28 November 2020

Available online 12 January 2021

0029-8018/Crown Copyright © 2021 Published by Elsevier Ltd. This is an open access article under the CC BY license (<http://creativecommons.org/licenses/by/4.0/>).

different types of ships evaluated each method by starting from their model test results to calculate the shaft power and propeller rate of revolution (ITTC, 1978). The 1978 ITTC Performance Prediction Method emerged as a result of comparing approximately one thousand sea trials to model test predictions and it is still in effect after going through several revisions.

Even though towing tank testing and extrapolation methods have been debated, discussed and improved over decades, there are inherent and well known shortcomings due to scale effects since model tests are carried out at Froude similarity while Reynolds similarity cannot be fulfilled simultaneously. In order to limit the effects of the shortcomings, towing tank facilities must rely on experience and large databases of both model tests and sea trials. Computational Fluid Dynamics (CFD) has been seen as an alternative to towing tank testing because of CFD's ability to fulfill both Froude and Reynolds similarities while providing a great deal of detail about the flow. However, the accuracy of CFD on prediction of full scale performance is still under concern. Even though several studies presented by Sun et al. (2020) and Niklas and Pruszek (2019) demonstrated that full-scale simulations can provide similar or better power predictions than towing tank experiments, the results from Reynolds Averaged Navier-Stokes (RANS) solvers in full scale is highly dependent on the computational set-up, e.g., the choice of turbulence model and modelling of hull roughness. The results of Lloyd's Register workshop on ship scale hydrodynamics (Ponkratov, 2016) also confirmed that differences between the numerical setups can lead to very diverse predictions on both power and propeller turning rate. Unlike the limited full scale verification and validation (V&V) studies mainly due to lack of full scale test data, assessment of state of the art in CFD methods in model scale has been a well established practice since 1980 Larsson et al. (2014). According to the resistance statistics of Larsson et al. (2014), the mean comparison error in per cent of the measured data value is  $-1.7\%$  and  $-1.3\%$  for KVLCC2 and KCS in fixed trim and sinkage condition while the standard deviations are  $1.3\%$  and  $1.2\%$  of the data value, respectively. It was also noted that the mean comparison error and standard deviation in self-propelled cases are considerably higher than those in the resistance cases (Larsson et al., 2014).

As identified by the Combined CFD/EFD Methods ITTC Specialist Committee, combination of EFD and CFD could be a feasible solution to increase the accuracy of power predictions instead of choosing EFD or CFD for the time being. If a part of the model testing or extrapolation procedure causes higher uncertainty than the numerical uncertainty and physical modelling errors of the CFD applications, accuracy will be increased. In the 1978 ITTC Performance Prediction method, the form factor has been identified by the Specialist Committee as one of the major causes of uncertainties, due to the Prohaska method (Prohaska,

1966) and scale effects on form factor for the determination of full scale resistance of ships. Form factor determination method suggested by Prohaska (1966) was recommended by 14th ITTC meeting (ITTC, 1975) when standardized performance prediction procedures were formulated and debated. During the formulation of the 1978 ITTC Power Prediction method, the form factor concept was found superior to 2-D methods such as the 1957 Power Prediction Method as it led to a better ship-model correlation (ITTC, 1978). The form factor determination method remained as the Prohaska method. However, the main issue with the Prohaska method was described by the ITTC as stated below:

"The problems of ships with partly submerged bulbous bows and the effects of wave breaking resistance for blunt bow forms need further consideration; in both cases it is probably advisable to lower the ... speed limits. Future developments for the determination of form factors on a more scientific basis is expected from the Resistance Committee" (ITTC, 1978)

In the 1978 ITTC Power Prediction method, the form factor concept of Hughes (1954) was adopted. It suggests that viscous resistance of a ship can be expressed in relation to a two-dimensional turbulent friction line and the form factor is independent of Reynolds number. As it will be explained in more detail in Section 2, the Prohaska method can be replaced by model scale double body CFD computations which is one of the least numerically complicated CFD applications since modelling of propulsors, free surface and roughness are omitted.

After the form factor determination method, the second error source was identified as the scale effects or speed dependency on form factor. When the 1978 ITTC method was accepted there has been substantial evidence on the scale effects on form factor with ITTC-57 line ITTC (1978). Further re-analysis of geosim test data performed by García Gómez (2000) and Toki (2008) confirmed the scale effects. Additionally, CFD studies performed by Pereira et al. (2017) showed that the speed dependency of form factors with the ITTC-57 line were larger than the numerical uncertainties. Terziev, Tezdogan and Incecik (2019) also showed that form factor is Reynolds number dependent and additionally suggested that the form factor varies with Froude number. The CFD investigations presented by Raven et al., 2008; Wang et al. (2015); Dogrul et al. (2020) and Korkmaz, Werner and Bensow (2019a) supported the existence of scale effects or speed dependency on form factor and indicated that the main cause of the scale effects are due to the 'ITTC 57 model-ship correlation line' rather than the hypothesis of Hughes (1954). CFD based form factor methods were investigated by Korkmaz et al. (2019a) and Wang et al. (2019) in further detail for sensitivity of form factor to grid density and type, speed dependency, presence of rudder, sinkage and trim. The latter investigation also demonstrated that CFD based form factors correlated better with the sea trials compared to the Prohaska method.

As a continuation of the initial study started by the Combined CFD/EFD Methods Specialist Committee, in this paper CFD based form factor methods have been investigated as an alternative method to the Prohaska method. KVLCC2 in design and ballast loading condition; KCS in design loading condition are computed at two speeds at both model and full scale. The model tests of KVLCC2 in ballast loading condition performed at SSPA's towing tank and the resistance data together with the measurement uncertainty analysis is presented for the first time in the literature. Wide range of CFD methods and setups are compared with the contribution from 9 different organisations and 7 different CFD codes. In order to quantify the sensitivity of different CFD approaches on form factor, non-ideal CFD setups are also computed and discussed. The scale effects on the form factor are presented by using the friction line proposed by Katsui et al. (2005) and numerical friction lines suggested by Korkmaz et al., 2019b in comparison to form factor based on the ITTC 57 model-ship correlation line.

The following research questions are aimed to be answered by this study.

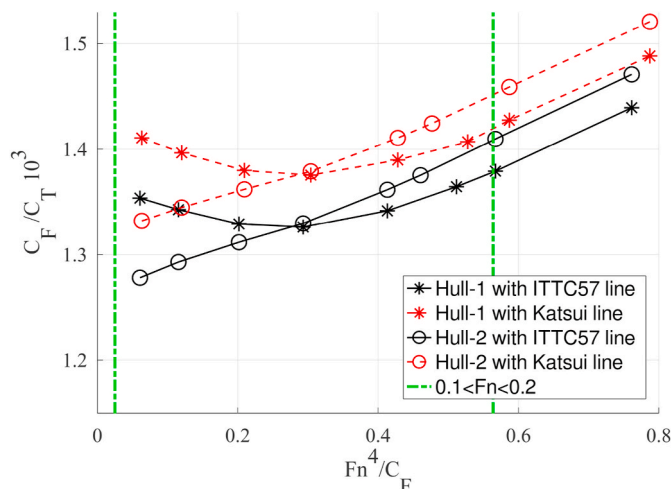


Fig. 1. Example of Prohaska plot in design loading condition.

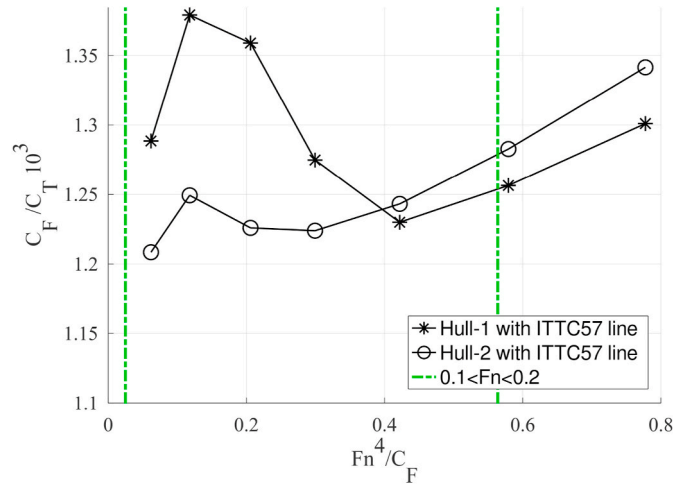


Fig. 2. Example of Prohaska plot in design ballast condition.

- Can CFD based form factors with state-of-the-art CFD codes be an alternative or supplement to the Prohaska method?
- Which CFD methods and setups are not fit for reliable CFD based form factor predictions?
- Can the scale effects on form factor be prevented?
- Should the full scale simulations replace the extrapolation methods for full scale resistance predictions?

This paper is structured as follows: Section 2 describes the background of the form factor concept and its determination by experimental methods. The flow solvers, numerical methods, computational domain and boundary conditions, procedure of CFD based form factor calculation are presented in Section 3. The computational conditions and details of the KVLCC2 towing tank tests in ballast condition are presented in Section 4. In Section 5, results and discussions are presented and conclusions are summarized in Section 6.

## 2. Background of the form factor concept and experimental determination methods

The form factor concept has been long discussed since the early 20<sup>th</sup> century. ITTC (1957) stated that ship resistance extrapolation based on three dimensional analysis (such as form factor approach) has been considered when the ITTC 1957 line was selected. In fact, some researchers believed that a two dimensional flow line is not sufficient for the extrapolation problem ITTC (1957), but rather that each hull form

requires a separate extrapolator such as Hughes (1954).

The definition of form factor as described by Hughes was adopted by the ITTC (1972) and it is still in practice. The wave-making resistance depends on the Froude number and at low speeds it becomes negligible for most hulls. Thus in carefully conducted experiments where care is taken with regard to turbulence stimulation, measurement accuracy at low speeds and good surface finish, a point in the  $C_T$  curve can be found. From this point towards smaller Froude numbers, the curve of  $C_T$  is ‘sensibly’ parallel to the two dimensional turbulent friction line. This is called by Hughes the ‘low Froude number run-in’ point (Hughes, 1954). The total resistance curve is formulated as,

$$C_T = C_F + C_{form} + C_W, \quad (1)$$

$$C_{form} = k C_F,$$

where  $C_F$  is the resistance equivalent to a flat plate in two dimensional flow,  $C_{form}$  is form resistance due to the shape of the hull,  $C_W$  is wave resistance and  $k$  is the form factor.  $C_{form}$  is proportional to  $C_F$  when the flow is turbulent and the given hull is smooth, streamlined (without separation) and in symmetrical form when towed in zero incidence angle.  $C_{form}$  is made up of components due to additional skin friction caused by curvature effects, flow in transverse directions and eddy-making (Hughes, 1954).

As Hughes (1954) described, form factor for a hull can be determined by the ratio  $C_T/C_F$  at the “run-in point” since the  $C_W$  is small enough be neglected in Eq. (1). However, in order to find the run-in point, the speed range for the resistance test must be extended to very low  $Fn$  and  $Re$  numbers which is rather challenging as the  $Re$  at such low speeds might be too low for turbulence stimulators to make sure the flow around the hull is turbulent. Additionally, certain scatter in resistance measurements at low speeds due to worsening measurement accuracy for small forces can hinder the form factor determination, as Lindgren and Dyne (1980) indicated.

As an alternative, Prohaska (1966) suggested a simple method to derive the form factor from resistance tests. When no separation is present, the form factor is expressed as

$$C_T = C_W + (1 + k)C_F. \quad (2)$$

The wave resistance coefficient,  $C_W$ , can be expressed as Eq. (3) which is the asymptotic expansion formula of wave-making resistance coefficient presented by Inui as cited in Toki (2008),

$$C_W = a \times Fr^4 + b \times Fr^8 + c \times Fr^{12} + d \times Fr^{16}. \quad (3)$$

$C_T$  at model scale is then expressed together with the Inui’s asymptotic expansion formula, Eq (3), as

$$C_{Tm} = (1 + k) \times C_F + C_W = (1 + k) \times C_F + a \times Fr^4 + b \times Fr^8 + c \times Fr^{12} + d \times Fr^{16}. \quad (4)$$

Table 1  
Participants and methods.

| Organisation                                  | Acronym     | Code      | ID | Turbulence model                                  | Wall model | Discretization |       | Grid Type |
|---|-------------|-----------|----|---|------------|----------------|-------|-----------|
|   |             |           |    |   |            | Type           | Order |           |
| CSHL University of Michigan                   | UM          | OpenFOAM  | 1  | Spalart-Allmaras, $k - \omega$ SST                | WF         | FV             | 2     | U         |
| China Ship Scientific Research Center         | CSSRC       | NaViiX    | 2  | RNG $k - \epsilon$                                | WF         | FV             | 2     | S         |
| Ecole Centrale de Nantes                      | ECN/CNRS    | ISIS-CFD  | 3  | EASM, $k - \omega$ SST                            | WF, WR     | FV             | 2     | U         |
| National Maritime Research Institute          | NMRI        | NAGISA    | 4  | EASM, $k - \omega$ SST                            | WF, WR     | FV             | 3     | OS        |
| Ocean, Coastal and River Engineering          | NRC-OCRE    | OpenFOAM  | 5  | $k - \omega$ SST                                  | WF         | FV             | 2     | U         |
| SSPA/Chalmers University of Technology        | SSPA/CTU    | SHIPFLOW  | 6  | EASM, $k - \omega$ SST                            | WR         | FV             | 2     | OS        |
| Shanghai Ship and Shipping Research Institute | SSSRI       | Star-CCM+ | 7  | $k - \omega$ SST, RSTM, Realizable $k - \epsilon$ | WF         | FV             | 2     | U         |
| Strathclyde University                        | Strathclyde | Star-CCM+ | 8  | $k - \omega$ SST                                  | WF         | FV             | 2     | U         |
| Yokohama National University                  | YNU         | SURF      | 9  | EASM, $k - \omega$ SST                            | WR         | FV             | 2     | S         |

FV Finite Volume; WR wall resolved; OS Overlapping Structured; S Single Block Structured; U Unstructured; WF wall functions.



**Table 2**  
Computational conditions.

| Computational conditions | $L_{PP}$ (m) | Scale factor | Draught at FP(m) | Draught at AP(m) | $S/L^2$ | $V_m$ (m/s) | $V_s$ (kn) | $Re_m$             | $Re_s$             | $Fn$  |
|--------------------------|--------------|--------------|------------------|------------------|---------|-------------|------------|--------------------|--------------------|-------|
| KVLCC2 (design)          | 320          | 58           | 20.8             | 20.8             | 0.2682  | 0.878       | 13         | $4.11 \times 10^6$ | $1.80 \times 10^9$ | 0.119 |
|                          |              |              |                  |                  |         | 1.047       | 15.5       | $4.90 \times 10^6$ | $2.14 \times 10^9$ | 0.142 |
| KVLCC2 (ballast)         | 320          | 45.714       | 8.6              | 11.4             | 0.1921  | 0.989       | 13         | $6.24 \times 10^6$ | $1.80 \times 10^9$ | 0.119 |
|                          |              |              |                  |                  |         | 1.179       | 15.5       | $7.44 \times 10^6$ | $2.14 \times 10^9$ | 0.142 |
| KCS (design)             | 230          | 31.6         | 10.8             | 10.8             | 0.1803  | 1.281       | 14         | $7.33 \times 10^6$ | $1.39 \times 10^9$ | 0.152 |
|                          |              |              |                  |                  |         | 2.196       | 24         | $1.26 \times 10^7$ | $2.39 \times 10^9$ | 0.260 |

Neglecting the higher order terms of Eq. (4) as they are close to zero at low Froude numbers and dividing each sides by  $C_F$ , the following linear relationship is obtained,

$$C_{Tm}/C_F \approx (1 + k) + a \times Fr^4/C_F. \quad (5)$$

Prohaska (1966) noted that when results of approximately 200 model tests have been plotted with Eq. (5), for  $Fn$  between 0.1 and 0.2, the  $C_T/C_F$  values for a great majority of the models plot on straight lines. One of the exceptions when the  $C_T/C_F$  values deviated from the straight line and points correlate with concave curves is with hull forms with  $C_B > 0.75$ . It was suspected that  $1 + k$  may be speed dependent, or as Prohaska (1966) stated “can be easily explained by as resulting from increasing trim on the bow.” The other hull form Prohaska observed where  $C_T/C_F$  values plot on convex curves was twin-screw models with appendages and for some models with full aft body lines, which was explained by a certain separation (Prohaska, 1966). It should be noted that detection of flow separation and treatment of deeply submerged transoms remain as challenges of the Prohaska method. However, the main weakness of the Prohaska method discussed in modern literature is the bulbous bow near the water surface and partly submerged bulbous bow in partial loaded conditions which is not mentioned by Prohaska (1966) since the model test data used by Prohaska dates back to 1966 and earlier when bulbous bows were not a popular design concept.

In order to illustrate this aspect of the uncertainty of form factor determination caused by the Prohaska method, the model test results of the resistance curves of two hulls are plotted as in Eq. (5) and presented in Fig. 1 and Fig. 2. In order to protect the confidentiality of the test results,  $C_T/C_F$  curves shown in Figs. 1 and 2 are slightly tilted without changing neither the general shape of the curves nor the relative position of each measurement point at the same Froude number. Hull-1 and Hull-2 are only different in bulbous bow and they are geometrically similar for the rest of the hull (95% identical hulls). The bulbous bow of Hull-1 features a mild goose-neck design (distinctly convex upper stem profile of the bulb) and has significantly more volume close to water surface at design loading condition compared to Hull-2. As can be seen from Fig. 1, not all  $C_T/C_F$  values of Hull-1 in design loading condition follow a straight line within the recommended  $Fn$  range, which is between 0.1 and 0.2 as indicated by the green vertical lines. The concave shape of  $C_T/C_F$  values for Hull-1 can be explained by the presence of significant and often steep waves that are generated by the bulb. The waves generated at significantly lower Froude numbers than the design speed are too short in wave length to favourably interact with the bow waves of the hull. On the other hand,  $C_T/C_F$  values of Hull-2 reasonably follow a straight line which suits the description of Prohaska (1966) since the waves are much smaller at low  $Fn$  as a result of reduced the pressure gradient and moving the bulb volume away from the water surface. Considering that the two hulls are 95% identical, large differences are observed in  $C_T/C_F$  curves.

The uncertainty with the Prohaska method further increases in the ballast loading conditions as shown in Fig. 2. The  $C_T/C_F$  values of Hull-1 within the recommended range shows a large hump which cannot be used for a line fit. In other words, the wave making resistance cannot be described by Eq. (4) and the linear relationship proposed by Prohaska in Eq. (5) is not valid. In ballast condition at the low speeds, Hull-2 also

shows a hump in  $C_T/C_F$  values which was not existent in the design condition. In order to demonstrate that a different friction line would not have helped, the  $C_T/C_F$  values are also calculated with the Katsui friction line (Katsui et al., 2005) instead of the 1957 ITTC model-ship correlation line. As seen in Fig. 1, the convex shape of the  $C_T/C_F$  values persists. As shown in this example, quantifying the uncertainty or error of Prohaska form factor determination method is difficult since it is very sensitive to the hull design. Considering that the bulbous bows are now a common feature of modern ship design, it is hard to advocate the validity and practicality of the Prohaska method for all hull designs and loading conditions.

One further aspect of uncertainty of form factor determination with the Prohaska method originates from the experimental uncertainty,  $U_D$ . The uncertainty on form factor can be significantly higher than the experimental uncertainty since it is not directly measured but obtained as a result of data reduction, i.e. regression analysis. This will be discussed thoroughly in Section 4 when the towing tank tests for KVLCC2 in ballast loading condition are presented.

### 3. Participants and methods

In total 9 different organisations with 7 different CFD codes contributed to the current study. The organisations are listed in Table 1 together with the main features of their methods. The results will be discussed and presented with the ID numbers of the organisations in the paper.

Two-equation turbulence models  $k - \omega$  SST, RNG  $k - \epsilon$ , Realizable  $k - \epsilon$  are used by the majority of the computations. Anisotropic models, EASM and RSTM, are not used by all organisations but EASM model is still covering a large portion of the calculations. Only one organisation used the one-equation Spalart-Allmaras model.

Simulations were performed using finite volume codes with 2nd order accurate schemes except one code with 3rd order accurate scheme. The grids used were single or multi-block structured grids (butt-joined, curvilinear or overlapping techniques) and unstructured ones.

Computational domain shape and size varies with each code. Majority of the upstream boundaries are located between  $1L_{PP}$  and  $1.5L_{PP}$  from the fore perpendicular (FP), but ECN/CNRS and SSPA/CTU are differing from others by using the distance of  $5L_{PP}$  and  $0.5L_{PP}$ , respectively. The downstream extent of the domains varied between  $8L_{PP}$  and  $0.8L_{PP}$  from the aft perpendicular (AP) while the common distance of downstream extent is between  $2L_{PP}$  and  $3L_{PP}$ . Lateral (both sideways and downwards) extend is commonly located between  $1.5L_{PP}$  and  $2.5L_{PP}$  away from the ship center-plane and free surface plane but two notable exceptions are  $1L_{PP}$  and  $4L_{PP}$  from UM and ECN/CNRS, respectively.

All computations were performed as double model with a symmetry boundary condition at the ship center-plane and free surface plane. Most popular upstream boundary condition is uniform in all variables with the exception of one participant with prescribed pressure. The downstream conditions are usually zero gradient in the streamwise direction except the pressure quantity that is specified. The lateral boundaries are dominated by far field boundary conditions but slip and zero gradient boundaries are also used. Majority of the computations (approximately 60%) are performed with wall resolved condition and the remaining

**Table 3**

Combination of uncertainty in measurement for resistance at  $Fn = 0.119$  and  $Fn = 0.142$ .

| Uncertainty Components         | Uncertainty at 16.0 °C |              |
|--------------------------------|------------------------|--------------|
|                                | $Fn = 0.119$           | $Fn = 0.142$ |
| Wetted area                    | 0.080%                 | 0.080%       |
| Speed                          | 0.067%                 | 0.057%       |
| Water temp.                    | 0.002%                 | 0.002%       |
| Dynamometer                    | 0.705%                 | 0.492%       |
| Repeat test, Deviation         | 0.470%                 | 0.344%       |
| Combined for single test       | 0.854%                 | 0.609%       |
| Repeat test, Deviation of mean | 0.210%                 | 0.154%       |
| Combined for repeat mean       | 0.743%                 | 0.525%       |
| Expanded for repeat mean       | 1.487%                 | 1.050%       |

simulations were performed with wall functions.

The CFD based form factor method considered for this study follows the assumptions of Hughes (1954) and is derived using the relation,

$$(1 + k) = \frac{C_F + C_{PV}}{C_{F0}} = \frac{C_V}{C_{F0}}, \quad (6)$$

where the frictional resistance coefficient ( $C_F$ ) and viscous pressure coefficient ( $C_{PV}$ ) are obtained by the double body CFD simulation.  $C_{F0}$  in the denominator of Eq. (6) is the equivalent flat plate resistance in two dimensional flow obtained from the same Reynolds number as the computations. In this study, three friction lines are considered: the ITTC-57 model-ship correlation line (ITTC, 1957), the Katsui line (Katsui et al., 2005) and numerical friction lines proposed by Korkmaz et al. (2019b). It is worth mentioning that the ITTC-57 line is not a pure friction line but it contains a component of form resistance (11.94% of the friction line of Hughes (1954)). It is included in the scope of the study because it is still the model to ship correlation line recommended by ITTC (2014a).

The shortcomings of the Prohaska method for the hulls with a pronounced bulbous bow have been mentioned in Section 2. In a case when there is just a small gap between the top of the bulb and the still-water surface, a flow separation may be generated around the top of the bulb for the double body simulations. Such flow separation would not occur in free-surface flow; therefore, the form factor obtained from the double body computation will be affected. Raven et al. (2008) suggested that if the bulb is submerged more by trimming the hull bow down, this issue can be prevented. Another drawback that is shared between CFD and EFD based form factor determination methods is the large submerged transom which may cause flow separation in the wake. The test cases used in this study do not possess the hull form features that may cause aforementioned issues for the CFD based form factor method. Therefore, no corrections have been applied to the double-body flow computations.

#### 4. Test cases and computational conditions

The two hulls used for the current study are:

**Table 4**

Total resistance coefficient,  $C_T$ , combined mean measurement uncertainty,  $U_D$ , number of repeat tests,  $N$ , at 16.0 °C.

| $Fn$  | $C_T \times 10^3$ | $U_D$ | $N$ |
|-------|-------------------|-------|-----|
| 0.110 | 3.981             | 0.84% | 4   |
| 0.119 | 3.968             | 0.74% | 5   |
| 0.133 | 3.976             | 0.60% | 4   |
| 0.142 | 4.001             | 0.52% | 5   |
| 0.147 | 4.016             | 0.51% | 4   |

- KVLCC2 with rudder
- KCS with rudder

The KVLCC2 and KCS hulls are designed at the Korea Research Institute for Ships and Ocean Engineering (KRISO) to be used as open test cases for CFD predictions. Extensive towing tank tests and CFD investigations were carried out in the last two decades. Therefore, hull lines and detailed hydrostatics are not presented. The hull and rudder geometries are obtained from Tokyo (2015) and SIMMAN (2008) workshops for KCS and KVLCC2, respectively.

The computational conditions for the study is presented in Table 2. Non-dimensional quantities,  $Re$  and  $Fn$ , are based on  $L_{pp}$ . The force coefficients are non-dimensionalized with the corresponding wetted surface coefficients,  $S/L^2_{PP}$ , to the loading conditions. For each hull and loading condition, two different speeds were used for the computations in order to investigate the importance and the effect of selecting a speed for the form factor determination. The first speed is chosen in the low side of the regular model testing speed range where  $C_T/C_F$  is close to the form factor (see Fig. 1) determined by the Prohaska method. The second speed is the design speed of each vessel. Data for resistance tests of KVLCC2 and KCS at design draught are adopted from Van et al. (2011). The resistance test data of the KVLCC2 in ballast loading condition has never been published. Therefore, SSPA determined a typical ballast loading condition for Very Large Crude Carriers (VLCC). Towing tank tests were performed at SSPA's towing tank including an uncertainty analysis of the resistance tests.

##### 4.1. Uncertainty analysis of KVLCC2 resistance tests in ballast draught

A KVLCC2 model with a scale factor of 45.714, made of the plastic foam material Divinycell, was manufactured with 5-axis CNC milling machine at SSPA. After the surface finishing and painting, the model was scanned with a 3D scanner to check the tolerances described in ITTC (2014c). A trip wire is mounted at 5% of  $L_{pp}$  aft from the fore perpendicular for the turbulence stimulation. The hull model is equipped with a dummy propeller hub and a rudder. The geometry of the rudder is obtained from SIMMAN (2008) and the dummy hub is a simple cylinder with the diameter of the boss end of the hull.

The model tests were performed in SSPA's towing tank which is 260 m long, 10 m wide and 5 m deep. The model tests were carried out in mid-May 2020. The total resistance, sinkage and trim were measured at Froude numbers varying between 0.110 and 0.147. The mid-sectional area of the KVLCC2 model in ballast loading condition is 0.155% of the towing tank section area. Therefore, no blockage correction is applied. The tests were started by performing one run per  $Fn = 0.119$  and  $Fn = 0.142$  speeds, respectively. It was followed by starting from the lowest  $Fn$  and the speed is increased successively at each run after 20 min of waiting time. There was a total of five repeat tests for  $Fn = 0.119$  and  $Fn = 0.142$ , while the rest of the speeds were repeated four times.

The uncertainty regarding the wetted surface area are quantified by measuring the model ballasting. The model and weights (calibrated 25 separate pieces) used for ballasting the model were weighted by two digital scales (ITTC, 2014b). Resulting uncertainties on the wetted surface are presented in Table 3 for  $Fn = 0.119$  and  $Fn = 0.142$  speeds.

The relative uncertainty of the towing speed is assessed by the bias limit of the towing carriage and they are presented in Table 3.

The water temperature during the tests showed less than 0.1 °C variation. As described in ITTC (2014b), the measured resistance is converted to 16.0 °C which was used for the CFD computations prior to the tests. The corresponding component of uncertainties in resistance due to temperature variation are presented in Table 3. The model was scanned and checked at the model workshop. The thermal deformation of the model is expected to be limited as the temperature difference between the model workshop and the towing tank is less than 5 °C.

An in-house design dynamometer with a sampling rate of 10 Hz was used for measuring the resistance. The measurement at each speed is

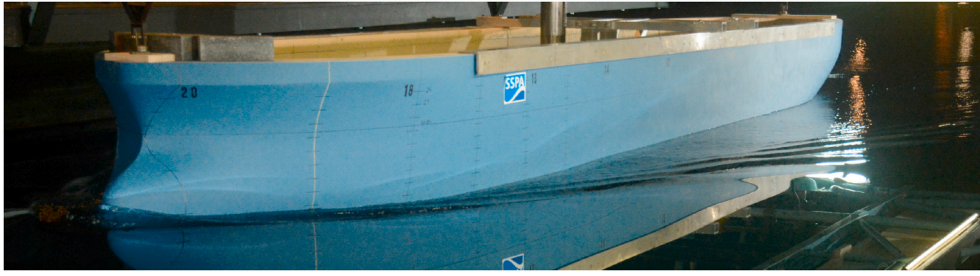


Fig. 3. KVLCC2 in ballast loading condition at  $Fn = 0.142$

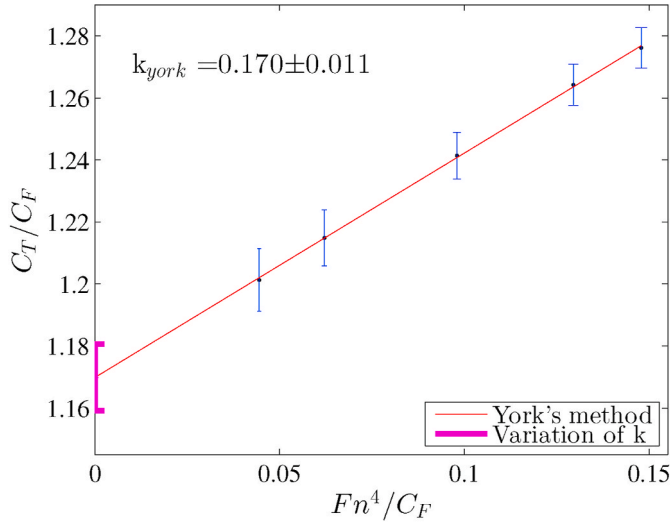


Fig. 4. Prohaska plot of KVLCC2 in ballast loading condition.

obtained by averaging the time history of the signal as described in ITTC (2014b). The standard uncertainty of average of the sampling history varied between 0.0008% and 0.0015%, while the average of all repetitions is 0.0011%. Therefore, the uncertainty of one reading from the Data Acquisition System (DAS) is negligible. The dynamometer available at the time of the towing tank tests were calibrated to a much greater range than the maximum model resistance. As a result, the uncertainty regarding to the dynamometer is the dominant source as can be seen in Table 3. The dynamometer calibration was checked after the tests. Additionally, a calibration with a range that was approximately 3 times the maximum model resistance was performed. The uncertainty due to the dynamometer dropped nearly three times with the smaller range which would have halved the total uncertainty in Table 3.

Based on the analysis described in ITTC (2014b), the significant components of uncertainties are combined through RSS (Root-Sum-Square). As seen in Table 3, major sources of the uncertainties are originating from the dynamometer (with the large calibration range) and the precision of measurement in the repeat tests. The uncertainty of resistance measurements for  $Fn = 0.119$  and  $Fn = 0.142$  are 0.74% and 0.53%, respectively. The expanded uncertainties in Table 3 correspond to the confidence level of 95%.

In Table 4, combined measurement uncertainties are presented in percent of the measured data value which is the mean total resistance of all repeat tests at each speed. The uncertainties are between 0.51% and 0.84%. As seen in Table 4, it is decreasing with increasing speed because at the high speeds the contribution from the dynamometer decreases.

As mentioned before, one aspect of uncertainty of form factor

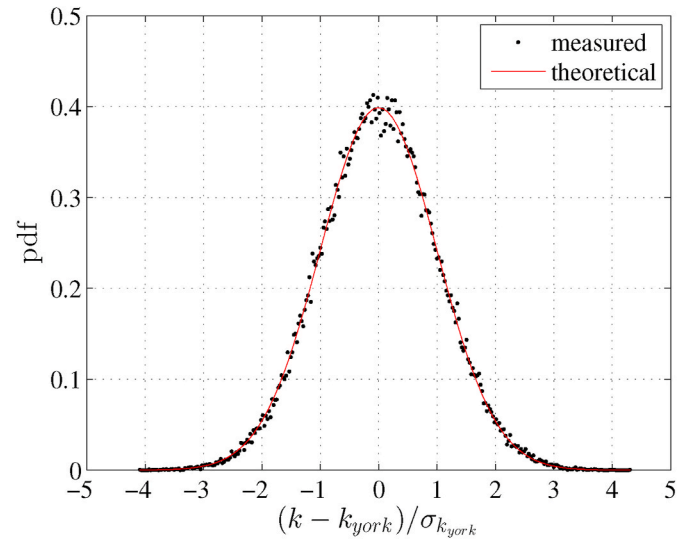


Fig. 5. Probability density function of the form factor of KVLCC2 in ballast loading condition.

determination with Prohaska method originates from the experimental uncertainty,  $U_D$ . In order to illustrate that the uncertainty on form factor is significantly higher than the experimental uncertainty, the Prohaska plot is presented in Fig. 4 with the error bars representing the experimental uncertainties presented in Table 4. Unlike the main discussion point in Section 2, the  $C_T/C_F$  values can be sensibly aligned to a line as the waves generated at the ballast loading condition were not too substantial as can be seen in Fig. 3.

The regression line in Fig. 4 is obtained by applying the method explained by York et al. (2004). This method considers the experimental uncertainties in the regression progress and predicts the uncertainties in the form factor as well. The resulting regression line is indicated as the York's method in Fig. 4 where the uncertainty on the form factor is illustrated with an error bar at  $Fn^4/C_F = 0$ . The uncertainty of form factor is calculated as 0.011.

Additionally a Monte Carlo simulation is performed to illustrate the variation on form factor due to measurement uncertainty. For each iteration, all measured point are varied as

$$C'_T = C_T + U_{SD} \times R \quad (7)$$

where  $C_T$  is measured point presented in Table 4,  $U_{SD}$  is the measurement uncertainty and  $R$  is normally distributed random number. In every iteration, a new regression line and form factor are calculated with the York et al. (2004) method. The error,  $k - k_{york}$ , obtained from the Monte Carlo simulation is normalized by the uncertainty obtained from

the York et al. (2004) method ( $\sigma_{\text{York}}$ ) and the probability density function (pdf) is calculated. As can be seen in Fig. 5, the Monte Carlo simulation indicates a normal distribution for the normalized error of the form factor and the standard deviation of the error is equal to the uncertainty obtained from the York et al. (2004) method. As a result of using both methods, the uncertainty of the form factor is calculated as 0.022 corresponding to 1.9% of  $1 + k$  for the 95% confidence interval.

## 5. Results

The analysis of approximately 300 double body simulations of the two hulls under the conditions stated in Table 2 is discussed in this section.

### 5.1. Friction and viscous pressure resistance in model scale

Firstly, friction and viscous pressure resistance coefficients are investigated since only these quantities are directly computed by CFD codes. Instead, form factor is a combination of the two computed values and a friction line. Therefore, detecting the tendencies between different CFD methods might be hindered due to errors cancelling each other.

#### 5.1.1. Uncertainty analysis

Uncertainty analysis is performed to quantify the grid uncertainty ( $U_G$ ) by SHIPFLOW and NAGISA codes. For the grid dependence study, five geometrically similar grids were used with the former code and systematically refined grid triplets are prepared for latter. Both SHIPFLOW and NAGISA performs the simulations in double precision in order to eliminate the round-off errors. The iterative uncertainties were quantified by the standard deviation of the force in percent of the average force over the last 10% of the iterations. Iterative uncertainty for  $C_F$  and  $C_{PV}$  were kept below 0.01% and 0.15% for SHIPFLOW, while iterative uncertainty for  $C_F$ ,  $C_{PV}$  and  $C_T$  for NAGISA were kept below 0.1% of their mean values for all simulations in model scale. Therefore, it was assumed that the numerical errors are dominated by the discretization errors and both iterative errors and round-off errors are neglected.

For SHIPFLOW, the procedure proposed by Eça and Hoekstra, 2014 was used to predict the grid uncertainties which are presented for the finest grid as a ratio of the computed value ( $U_G\%S_1$ ) in Table 5. In order to quantify the grid uncertainty for NAGISA, three criteria are adopted, e.g. Factor of Safety (FS) method proposed by Xing and Stern (2009), Correction Factor (CF) method and Grid Convergence Index (GCI) method shown in ITTC (2017). Table 6 summarizes the results for KVLCC2 in design and ballast loading condition and KCS. In the cases where monotonic convergence is not obtained, the solution change is less than 1% of  $S_1$  ( $\varepsilon_{21}\varepsilon_{32}$ ). Therefore,  $U_G$  is omitted and noted with a "-" symbol in Table 6.

**Table 5**

Estimated grid uncertainties of SHIPFLOW for KVLCC2 and KCS in model scale for EASM and  $k-\omega$  SST turbulence models, in percentage of the computed result of the finest grid  $S_1$ .  $U_{C_T} = U_{C_F} + U_{C_{PV}}$ .

| $U_G$    | Turbulence model | KVLCC2 (design) |       | KVLCC2 (ballast) |       | KCS (design) |      |
|----------|------------------|-----------------|-------|------------------|-------|--------------|------|
|          |                  | Fn              |       | Fn               |       | Fn           |      |
|          |                  | 0.119           | 0.142 | 0.119            | 0.142 | 0.152        | 0.26 |
| $C_F$    | EASM             | 1.0             | 1.2   | 1.3              | 1.2   | 3.5          | 3.2  |
|          | $k-\omega$ SST   | 1.1             | 1.4   | 0.9              | 1.0   | 5.9          | 9.6  |
| $C_{PV}$ | EASM             | 1.0             | 3.0   | 17.9             | 5.1   | 32.5         | 19.4 |
|          | $k-\omega$ SST   | 1.1             | 3.0   | 23.0             | 10.8  | 30.2         | 21.0 |
| $C_T$    | EASM             | 1.0             | 1.6   | 3.6              | 1.8   | 6.7          | 5.0  |
|          | $k-\omega$ SST   | 1.1             | 1.7   | 3.7              | 2.3   | 8.4          | 10.7 |

**Table 6**

Estimated grid uncertainties ( $U_G$ ) of NAGISA for KVLCC2 and KCS in model scale for EASM turbulence model, in percentage of the computed result of the finest grid  $S_1$ .

| U <sub>G</sub>  | Method | KVLCC2   | KVLCC2    |       | KCS      |
|-----------------|--------|----------|-----------|-------|----------|
|                 |        | (design) | (ballast) |       | (design) |
|                 |        | Fn       | Fn        | Fn    | Fn       |
|                 |        | 0.142    | 0.119     | 0.142 | 0.26     |
| C <sub>F</sub>  | FS     | 3.1      | 2.1       | 2.0   | –        |
|                 | CF     | 3.8      | 2.4       | 2.3   | –        |
|                 | GCI    | 0.3      | 1.2       | 1.2   | –        |
| C <sub>PV</sub> | FS     | 0.1      | –         | –     | 4.7      |
|                 | CF     | 0.1      | –         | –     | 5.1      |
|                 | GCI    | 0.1      | –         | –     | 3.0      |
| C <sub>T</sub>  | FS     | –        | 0.3       | 0.3   | –        |
|                 | CF     | –        | 0.2       | 0.2   | –        |
|                 | GCI    | –        | 0.2       | 0.2   | –        |

#### 5.1.2. Statistics of $C_F$ and $C_{PV}$

The simulations in model scale comprise computations from seven different codes and six different turbulence models with wall functions and wall resolved approaches. These computations include not only the CFD setups according to the best practice guidelines (BPG) or standard settings but also setups that deviated from recommended guidelines since one of the aim of this study is to identify the methods that are not well suited for the form factor determination. In order to differentiate the contribution of the computations with deliberately made undesired settings, two different populations are considered when the statistics, such as mean and standard deviation, are calculated. The first population (denoted as P1) includes all simulations and the second population (denoted as P2) is the computations performed with best practices or standard settings of each code. It was deemed necessary to add one more population as a sub-population of the latter because of concerns on the statistics being biased by a code significantly outnumbering others in some test cases. Therefore, the third population (denoted as P3) is obtained by selecting the computations from the two finest grids of each code per CFD approach such as turbulence model, wall treatment. This selection is based on the number of cells under the assumption that fine grids have less discretization uncertainty.

The mean and standard deviation of  $C_F$  and  $C_{PV}$  for each condition is calculated with the three previously mentioned populations. As presented in Table 7 and Table 8, it is observed that statistics of different populations of the same condition showed limited variation except KVLCC2 in design condition which is the condition many of the deliberate variations were applied to CFD setups. In Fig. 6, the Population 2 and simulations with non-desired CFD set-ups are visualised by dividing all the computations for KVLCC2 in design condition into two groups: computations with non-standard CFD set-ups, and simulations with the best practice guidelines (BPG) or standard CFD set-ups. The small difference in statistics between the Population 2 and 3 shows that the statistics are not biased even though some test cases are overcrowded

**Table 7**

The mean and standard deviation of  $C_F$  for KVLCC2 and KCS in model scale.

| Quantity      | KVLCC2 (design) |       | KVLCC2 (ballast) |       | KCS (design) |       |
|---------------|-----------------|-------|------------------|-------|--------------|-------|
|               | Fn              |       | Fn               |       | Fn           |       |
|               | 0.119           | 0.142 | 0.119            | 0.142 | 0.152        | 0.26  |
| Mean (P1)     | 3.462           | 3.381 | 3.298            | 3.21  | 3.112        | 2.893 |
| Mean (P2)     | 3.47            | 3.394 | 3.298            | 3.215 | 3.105        | 2.892 |
| Mean (P3)     | 3.455           | 3.376 | 3.298            | 3.215 | 3.095        | 2.885 |
| $\sigma$ (P1) | 2.7%            | 2.5%  | 2.5%             | 2.4%  | 2.0%         | 1.6%  |
| $\sigma$ (P2) | 2.5%            | 2.6%  | 2.5%             | 2.5%  | 2.0%         | 1.6%  |
| $\sigma$ (P3) | 2.9%            | 2.8%  | 2.5%             | 2.6%  | 1.9%         | 1.8%  |

P1 Population 1; P2 Population 2; P3 Population 3.



**Table 8**The mean and standard deviation of  $C_{PV}$  for KVLCC2 and KCS in model scale.

| Quantity      | KVLCC2 (design) |       | KVLCC2 (ballast) |       | KCS (design) |       |
|---------------|-----------------|-------|------------------|-------|--------------|-------|
|               | Fn              | Fn    | Fn               | Fn    | Fn           | Fn    |
|               | 0.119           | 0.142 | 0.119            | 0.142 | 0.152        | 0.26  |
| Mean (P1)     | 0.793           | 0.777 | 0.504            | 0.494 | 0.387        | 0.33  |
| Mean (P2)     | 0.789           | 0.739 | 0.501            | 0.49  | 0.387        | 0.326 |
| Mean (P3)     | 0.794           | 0.745 | 0.499            | 0.488 | 0.393        | 0.335 |
| $\sigma$ (P1) | 9.2%            | 13.1% | 6.6%             | 6.2%  | 7.6%         | 13.6% |
| $\sigma$ (P2) | 9.7%            | 9.8%  | 7.3%             | 6.9%  | 9.0%         | 14.4% |
| $\sigma$ (P3) | 10.2%           | 10.3% | 7.9%             | 7.5%  | 9.2%         | 15.0% |

with simulations from one code. The computations performed with the best practices or the standard settings of each code (Population 2) will be used for the rest of the analysis, except when the results of deliberate variations of CFD setups are discussed.

**Friction and viscous pressure resistance coefficients.**  $C_F$  and  $C_{PV}$  in model scale for KVLCC2 in both loading conditions and KCS in design condition are presented versus grid size (in logarithmic scale) in Fig. 7

and Fig. 8. In order to have references for the friction resistance coefficient, the ITTC-57 line and the Katsui line are plotted in Fig. 7.

As can be seen in Figs. 7 and 8, there is no distinct dependence of results on the grid size. Note that this is a comparison of unsystematically varied methods and grids. However, other dependencies such as the turbulence modelling and the wall treatment were found both on  $C_F$  and  $C_{PV}$ . The frictional resistance coefficients from UM (Participant 1) and SSPA/CTU (Participant 6) indicate a strong dependence on turbulence model while this effect is rather limited on the results of ECN/CNRS (Participant 3), NMRI (Participant 4) and YNU (Participant 9). The viscous pressure coefficients from ECN/CNRS and SSPA/CTU show larger dependence on turbulence models than the others. ECN/CNRS and NMRI performed simulations both with wall resolved and wall function. Both codes indicate a significant dependence on wall treatment especially for  $C_F$  but also for  $C_{PV}$  which is less sensitive to the wall treatment than the frictional resistance component.

**Variations of CFD setups.** The previously mentioned CFD setups that varied from recommended guidelines on KVLCC2 in design condition have been applied by UM, ECN/CNRS, SSPA/CTU and SSSRI. UM (Participant 1) varied grids focusing specifically to the grid resolution near the wall using two turbulent models. As can be seen in Fig. 9, where

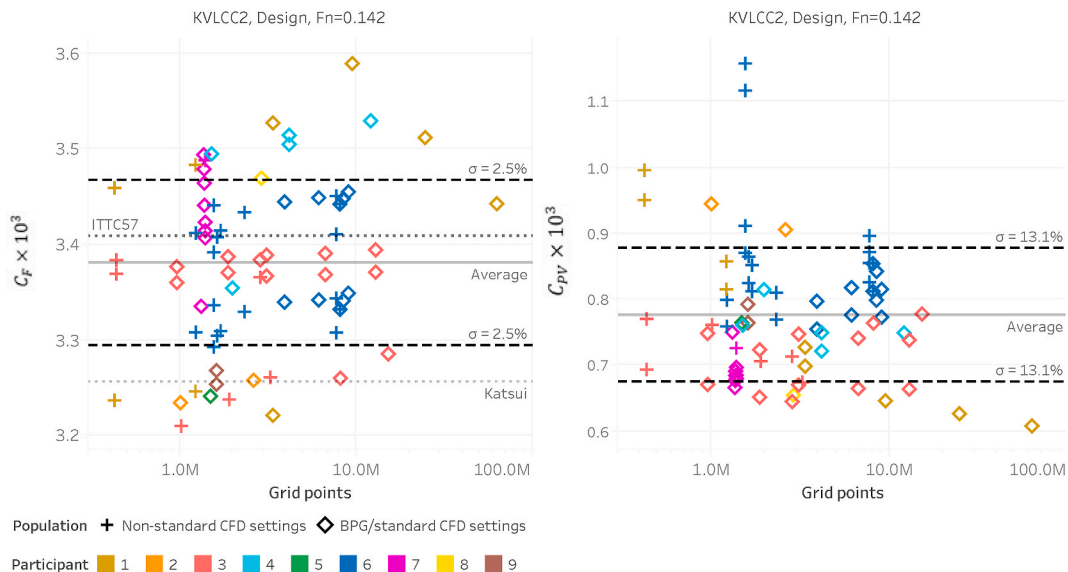


**Fig. 6.** Frictional coefficient (left) and viscous pressure coefficient (right) in model scale for KVLCC2 hull in design loading condition at  $Fn = 0.142$

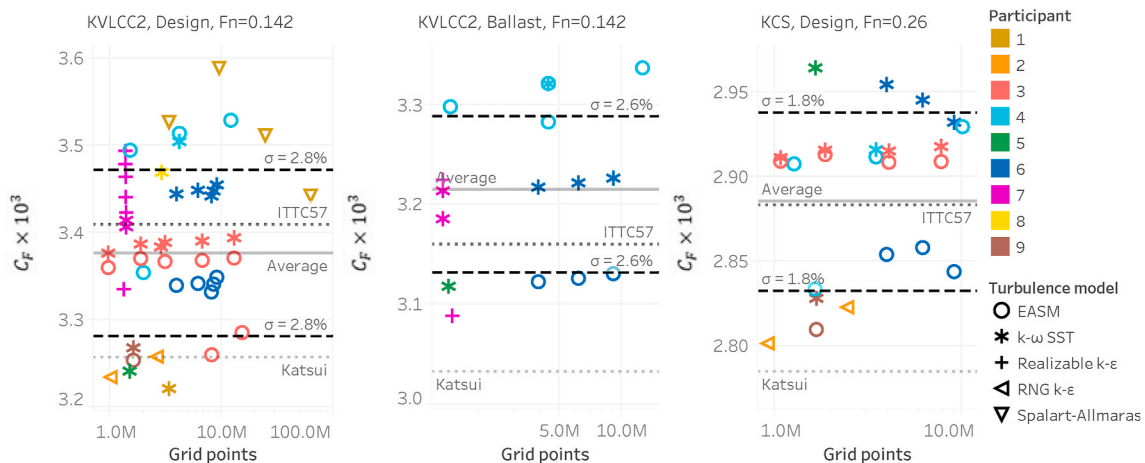


**Fig. 7.** Frictional coefficient,  $C_F$ , in model scale for KVLCC2 hull in design loading condition at  $Fn = 0.142$  (left), KVLCC2 in ballast loading condition  $Fn = 0.142$  (center) and KCS hull in design loading condition at  $Fn = 0.26$  (right).



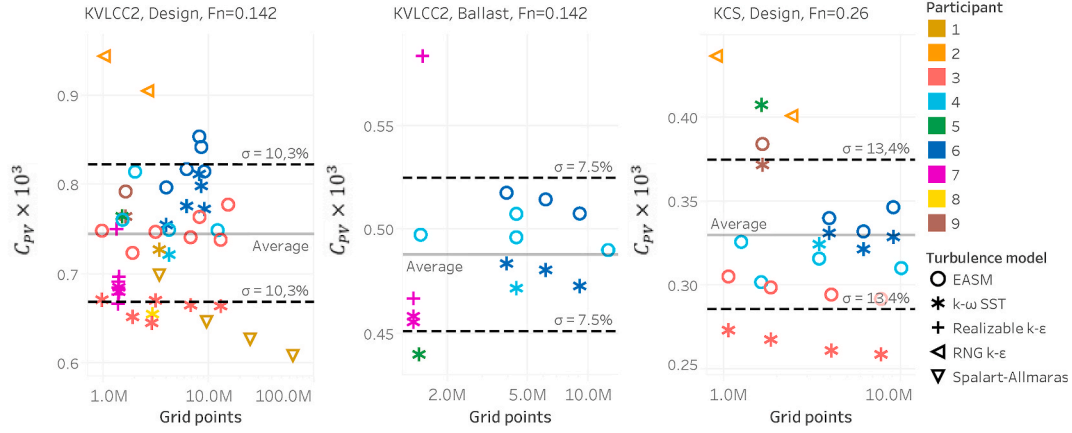


**Fig. 8.** Viscous pressure coefficient,  $C_{PV}$ , in model scale for KVLCC2 hull in design loading condition at  $Fn = 0.142$  (left), KVLCC2 in ballast loading condition  $Fn = 0.142$  (center) and KCS hull in design loading condition at  $Fn = 0.26$  (right).

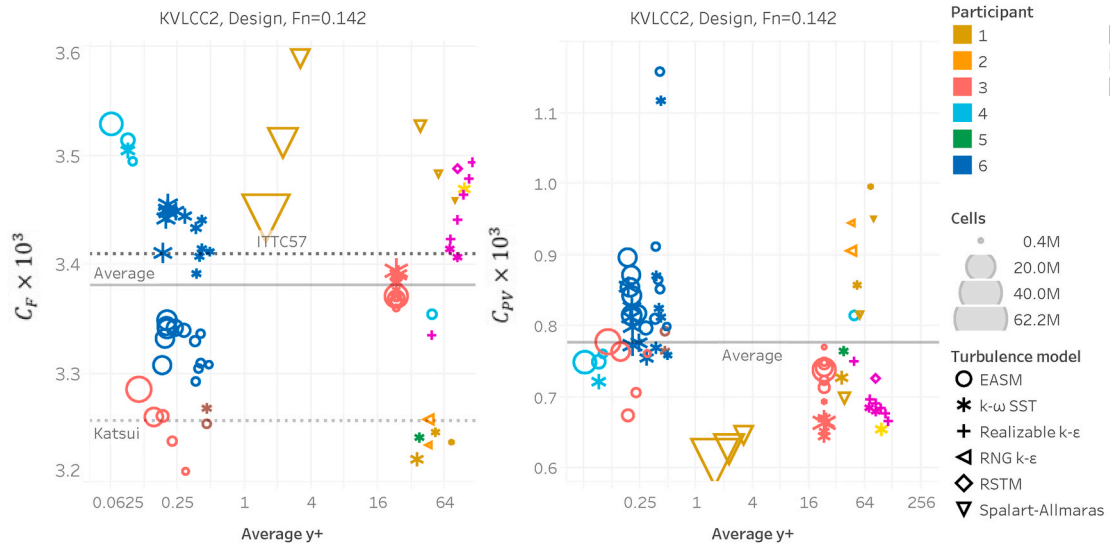


**Fig. 9.**  $C_F$  (left) and  $C_{PV}$  (right) in model scale for KVLCC2 hull in design loading condition at  $Fn = 0.142$  against mean  $y^+$ .  $y^+ < 1$ : wall resolved,  $y^+ > 1$ : wall function.

all computations on KVLCC2 in design condition are presented,  $k-\omega$  SST and Spalart-Allmaras turbulence models shows high sensitivity on  $C_F$  to both grid refinement and  $y^+$  variation. However, the variation on  $C_{PV}$  is limited except for the coarsest grid set.

ECN/CNRS (Participant 3) performed grid variations also with adaptive grid refinement. When wall functions were used,  $C_F$  and  $C_{PV}$  showed small variation even for the very coarse grids. However, wall resolved simulations of ECN/CNRS are more grid dependent compared to wall functions. This is explained by the increasing grid resolution near the wall rather than the increase in grid size for the wall resolved computations.

In addition to the systematic grid variations for the grid dependence studies, SSPA/CTU (Participant 6) performed grid variations by coarsening the grid of the bow and the stern region of the KVLCC2 hull in the longitudinal direction while keeping the rest of the grid the same. For this exercise, the second finest grid and the coarsest grid of the grid dependence study was selected as a starting point. Coarsening the bow and stern regions up to grid density of one third of the starting grids did not show a significant variation on  $C_F$  but some variation in  $C_{PV}$  for the same turbulence model except for one case. When the coarsest grid was further coarsened in the aft, the  $C_{PV}$  was calculated extremely high as seen in Fig. 6 (highest two values from Participant 6) while the variation

of  $C_F$  was limited. The grid variations of SSPA/CTU on KVLCC2 showed that when the grid resolution normal to the wall is kept similar,  $C_F$  and  $C_{PV}$  are more sensitive to the grid density in aftbody than forebody.

Simulations of SSSRI (Participant 7) was performed with three different turbulence models. As can be seen from Fig. 9, both  $C_F$  and  $C_{PV}$  obtained from Reynolds Stress Turbulence Model (RSTM) were significantly higher than the realizable  $k-\epsilon$  and  $k-\omega$  SST models with similar grids and average  $y^+$  values. Additionally, different types of wall functions were used with realizable  $k-\epsilon$  and  $k-\omega$  SST models while keeping the grids similar.  $C_F$  and  $C_{PV}$  showed only marginal change due to different wall function type for the  $k-\omega$  SST model. However, the realizable  $k-\epsilon$  model showed a substantial variation in both  $C_F$  and  $C_{PV}$  due to different wall function treatment. Finally,  $y^+$  is varied with the realizable  $k-\epsilon$  model. It is observed that when the average  $y^+$  increases (from 71 to 112 in steps of 11),  $C_F$  also increases up to 2% while  $C_{PV}$  decreases up to 4.5% as shown in Fig. 9. Therefore, a significant dependence of  $y^+$  and wall function treatment on viscous resistance is observed with the realizable  $k-\epsilon$  model.

## 5.2. CFD based form factors with the ITTC-57 line

CFD based form factors are calculated using Eq. (6) and presented

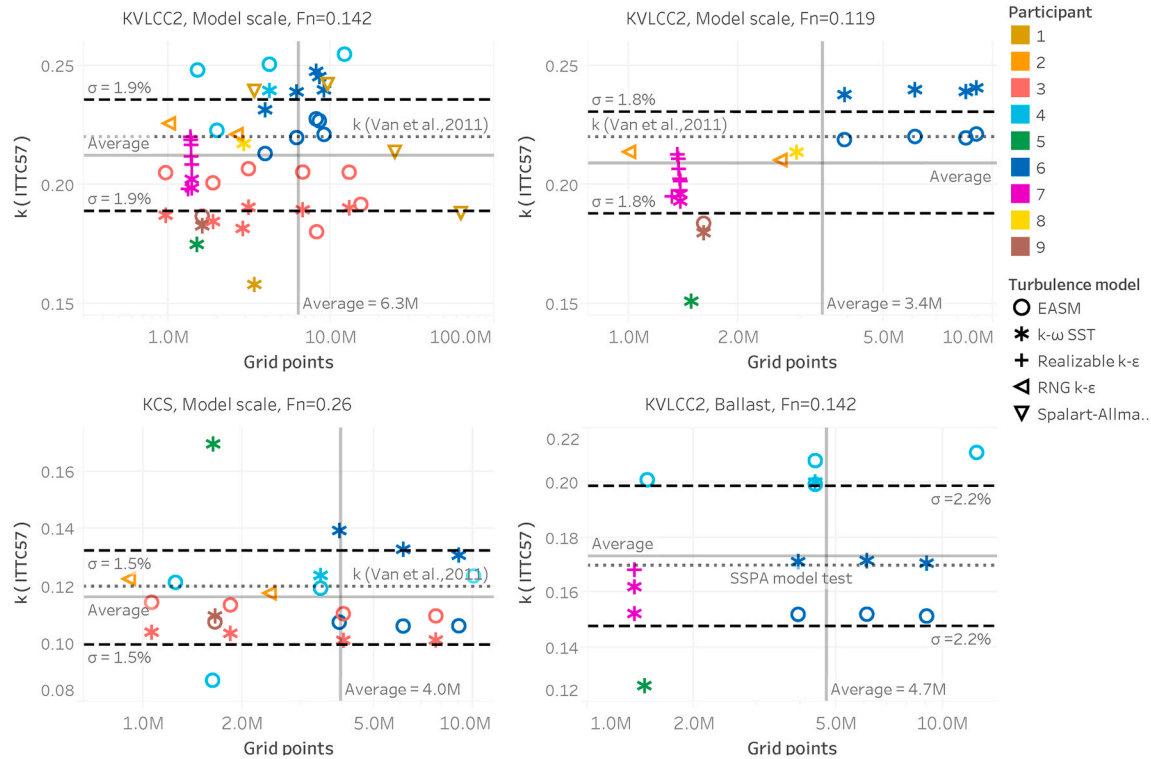


**Fig. 10.** Form factor,  $k$ , based on ITTC-57 line versus grid size for KVLCC2 hull in design loading condition at  $Fn = 0.142$  (top left) and  $Fn = 0.119$  (top right), KCS hull in design loading condition at  $Fn = 0.26$  (bottom left) and KVLCC2 in ballast loading condition  $Fn = 0.142$  (bottom right).

versus the number of grid points in Fig. 10. Note that only the simulations performed according to the best practice guidelines or standard settings of each code are presented and logarithmic scale is used in the grid points axis for better clarity. In addition to standard deviation in percentage of  $(1 + \bar{k})$  and mean of the CFD based form factors ( $\bar{k}$ ), form factors determined by model tests of Van et al. (2011) for KVLCC2 and KCS in design condition and KVLCC2 in ballast loading condition of SSPA are plotted in Fig. 10.

Mean of the form factor predictions for the KVLCC2 in design condition at  $Fn = 0.119$  and  $Fn = 0.142$  are both close to the form factor determined experimentally. The standard deviation of the form factors obtained from the unsystematically varied methods and grids at both speeds is around 1.9%. If the form factor is used in extrapolation of the model resistance value for this KVLCC2 case, this would cause approximately 3% spread in the predicted full-scale resistance (roughness, correlation allowance and air resistance excluded). Number of grid cells among the computations varied between one million to 62 million. However, form factor predictions do not indicate dependence on the number of grid cells.

Mean of the form factor predictions for the KCS in design condition at  $Fn = 0.26$  is very close to the experimental value. However, at  $Fn = 0.152$ , the mean value of form factor is 0.015 smaller than the mean form factor at  $Fn = 0.26$  as shown in Table 9 in Section 5.3. This difference was not as large for the KVLCC2 because the  $Re$  difference between the speeds were small (19%). However,  $Re$  difference between the speeds for the KCS hull is 71% which is big enough to reveal the speed dependency of the form factor as it is discussed in further detail in Section 5.3. The standard deviation of 1.5% translates to approximately 1% in full scale resistance excluding the contribution of roughness, correlation allowance and air resistance. Note that this is a remarkable result even though such a wide range methods and grids were used since KCS like hulls are the ones that suffers the most from the Prohaska method because of the prominent bulb designs.

All the computations for KVLCC2 in ballast case had to be performed prior to the model tests. The slight discrepancy in water temperature

between computations and tests were corrected using ITTC (2014b) procedures for form factor determination. Form factor predictions for the KVLCC2 in ballast loading condition showed a similar standard deviation to the other cases. However, the mean value of the form factor is not as close to the experimentally determined form factor as the other cases. As explained in Section 4, uncertainty analysis was performed for the form factor. When the uncertainty of the Prohaska method on the experimentally determined form factor is considered, majority of the simulations are still within the uncertainty range.

It is observed in Fig. 10 that some form factor predictions are relatively far from the experimentally derived form factor. However, it is encouraging to observe that there are some consistent patterns for most of the codes. The form factor was under-predicted similarly by YNU (Participant 9) and ECN/CNRS (Participant 3) for both KVLCC2 and KCS hulls in design condition. Results of SSSRI (Participant 7) are also under-predictions for all the cases. It should be noted that as long as one code with a certain set-up consistently predicts the form factor with the same tendency, application of correlation factors ( $C_P$  or  $C_A$ ) in the 1978 ITTC Power Prediction method will help to reduce the discrepancies.

**CFD Code Dependency.** The dependencies and tendencies of each code for the form factor predictions are plotted in Fig. 11 and Fig. 12. Computations from each code are stacked in separate columns where box-and-whisker plots are placed with markers. The box plot can be identified with the gray color and sized with the lower and upper quartiles. Lines extending from the boxes (whiskers) extend to the data within 1.5 times the interquartile range (IQR). The markers are colored with the turbulence models, shaped according to the wall treatment type and sized according to the number of cells.

**Turbulence Model Dependency.** The choice of turbulence model stands out as a decisive element of the CFD based form factors when the results of UM, ECN/CNRS, NMRI and SSPA/CTU are considered. Even if the same code and similar CFD set-ups are used, a significant dependence on turbulence models are observed. However, a general trend for each turbulence model cannot be maintained either. For example, ECN/CNRS (Participant 3), NMRI (Participant 4) and YNU (Participant 9)

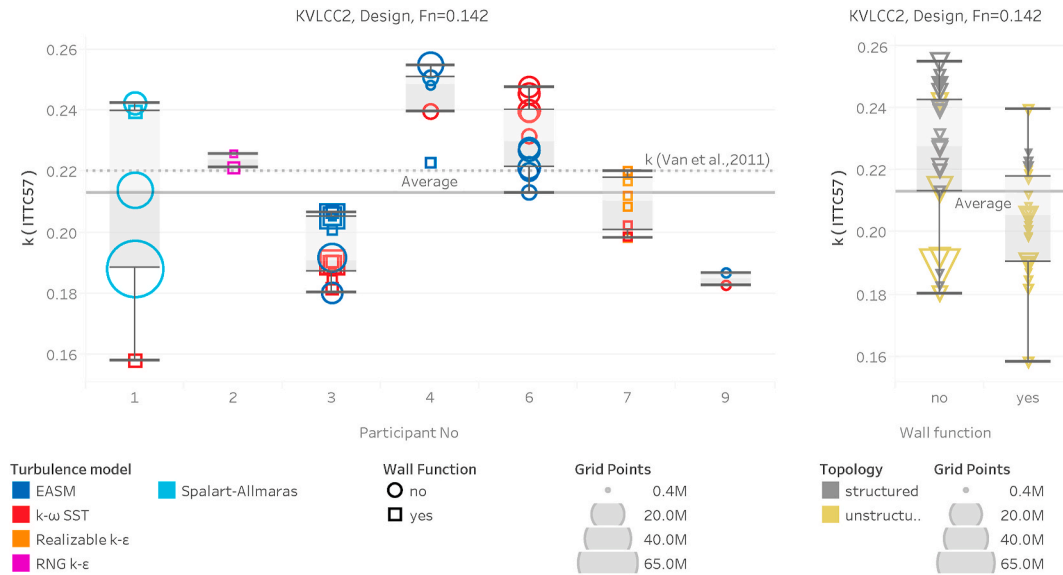


Fig. 11. Tendency of CFD codes and methods for form factors,  $k$ , based on ITTC-57 line for KVLCC2 hull in design loading condition at  $Fn = 0.142$ .

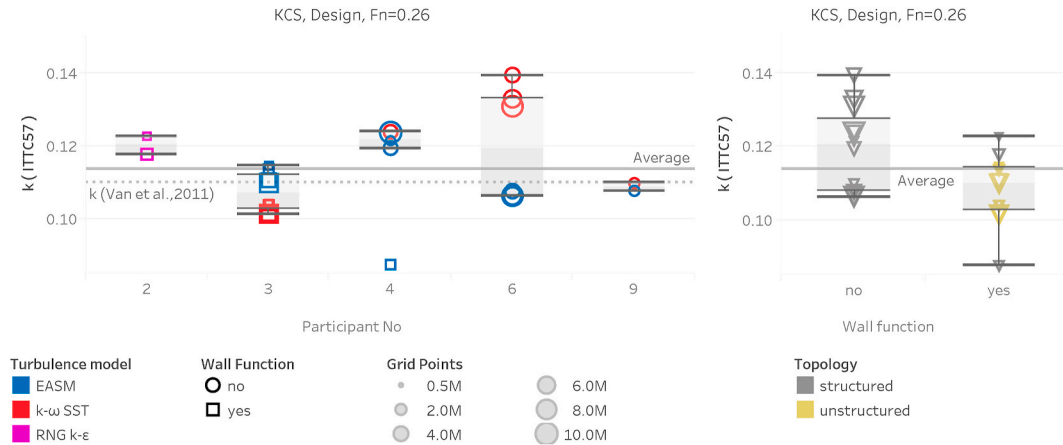


Fig. 12. Tendency of CFD codes and methods for form factors,  $k$ , based on ITTC-57 line for KCS hull in design loading condition at  $Fn = 0.26$ .

predicted higher form factors with EASM turbulence model than with  $k - \omega$  SST, while this is the opposite with SSPA/CTU (Participant 6). It should be also noted that the form factor predictions from the same turbulence model with different CFD codes are largely scattered. Therefore, the dependence of form factors to the CFD codes surpasses the choice of the turbulence model.

**Wall Treatment Dependency.** The type of wall treatment and  $y^+$  can be considered as significant dependencies of form factor as it was the case for  $C_F$  and  $C_{PV}$  investigated earlier. ECN/CNRS and NMRI performed computations with the same turbulence models of  $k - \omega$  SST and EASM and also both participants had simulations with and without wall functions. As can be seen from Figs. 11 and 12, form factor dependence on the wall treatment is observed with both ECN/CNRS (Participant 3) and NMRI (Participant 4), while a significant dependence on  $y^+$  was observed with the realizable  $k - \epsilon$  model for SSSRI.

On the right side of Figs. 11 and 12, simulations from all codes are sorted with the type of wall treatment. The markers are colored with the type of the grid. The box plots of both KVLCC2 and KCS indicate that interquartile range (IQR) of simulations with wall functions are smaller than wall resolved. However, the distance between the whiskers are similar for both approaches. Although the CFD results as a whole are a product of unsystematically varied methods and grids, the comparison of median values of different wall modelling indicates that simulations

with wall functions predict considerably smaller form factors compared to wall resolved approach.

### 5.3. Form factors with alternative friction lines

As mentioned earlier in Section 1, speed dependency or scale effects have been found on the form factor by the previous investigations. However, it should be noted that the form factors should always be considered with the friction line used as the physical meaning of speed dependency or scale effects on the form factor is that the viscous resistance of a ship is not proportional to the selected friction line. Even if the concept of Hughes (1954) (see Section 2) is true, different sizes of geomim models and double body simulations at different Reynolds numbers will result in different form factors as a result of using an ‘improper’ friction line. The currently recommended friction line, the ITTC-57 line (ITTC, 1957), is in fact not a pure friction line as Hughes (1954) hypothesis requires but a model-ship correlation line. Therefore, speed dependency of the form factors with ITTC-57 line is not extraordinary but expected.

Instead of the ITTC-57 line,  $C_{F0}$  in Eq. (6) can be replaced by other friction lines such as Katsui et al. (2005) or numerical friction lines (NFL) that are derived by using the same code as the double body simulations. Prior to this study, only SSPA/CTU obtained a NFL with the

**Table 9**

Statistics of the form factor predictions with ITTC-57 line (I), Katsui line (K) and numerical friction lines (N).

| Quantity     | KVLCC2 (design) |       | KVLCC2 (ballast) |       | KCS (design) |       |
|--------------|-----------------|-------|------------------|-------|--------------|-------|
|              | Fn              | Fn    | Fn               | Fn    | Fn           | Fn    |
|              | 0.119           | 0.142 | 0.119            | 0.142 | 0.152        | 0.260 |
| Mean (I)     | 0.212           | 0.223 | 0.175            | 0.181 | 0.102        | 0.117 |
| Mean (K)     | 0.271           | 0.280 | 0.227            | 0.231 | 0.149        | 0.156 |
| Mean (N)     | 0.296           | 0.296 | 0.242            | 0.243 | 0.163        | 0.165 |
| $\sigma$ (I) | 1.5%            | 1.6%  | 2.1%             | 2.0%  | 1.3%         | 1.2%  |
| $\sigma$ (K) | 1.5%            | 1.6%  | 2.1%             | 2.0%  | 1.3%         | 1.2%  |
| $\sigma$ (N) | 2.4%            | 2.1%  | 1.8%             | 1.9%  | 0.7%         | 0.8%  |

SHIPFLOW code for EASM and  $k - \omega$  SST turbulence models (Korkmaz et al., 2019b). Since other participants did not have numerical friction lines, frictional resistance coefficients of infinitely thin 2D plates were computed by NMRI, SSSRI, Strathclyde and YNU with the same turbulence models, wall treatment and Reynolds number as the corresponding double body simulations. These  $C_F$  values obtained from the flat plate simulations were then used as  $C_{F0}$  in Eq. (6) for the form factor determination.

Form factors based on the ITTC-57 line and the Katsui line are also calculated using the same simulations where NFL data is available. The mean values and the standard deviations of the form factors based on different friction lines are presented in Table 9. The speed dependency can be identified by comparing the mean of the form factor predictions of different Reynolds numbers at the same loading condition. As expected, speed dependency of form factors with the ITTC-57 line is observed for the both hulls and the loading conditions. The largest speed dependency, however, is observed for the form factors of the KCS hull with the ITTC-57 line as the difference between the Reynolds numbers is the greatest among other cases. The speed dependencies are reduced considerably when the Katsui line is used and they are almost completely eliminated with numerical friction lines for all test cases.

Regardless of an existence of speed dependency of form factors, the choice of speed from which the form factor will be determined is a relevant issue for CFD computation. The extrapolated full scale viscous resistance predictions will be influenced by the choice of the model scale speed when the speed dependency exists. Therefore, the speeds that correlates better with the experimentally determined form factors should be preferred. Based on the form factor predictions presented in Table 9, design speeds of KVLCC2 and KCS are suggested if the ITTC-57 line is used for the form factor determination. Another point of concern is choosing the speed that provides the smaller numerical uncertainties and modelling errors. The grid uncertainties presented in Tables 5 and 6 for SHIPFLOW and NAGISA codes showed limited change of grid uncertainties with the speed while the change of  $U_G$  were not systematically increasing or decreasing. In terms of modelling errors, numerical

transition from laminar to turbulent flow can be concerning when the  $Re$  is too low as this phenomenon occurs even without the use of transition turbulent models as shown in Eça and Hoekstra, 2008 and Korkmaz et al. (2019b).

As presented in Table 9, the mean of form factors with ITTC-57 line greatly differs from Katsui line and NFL. The physical explanation of this observation is that when ITTC-57 line is used, the form resistance (see Section 2) is significantly under-predicted due to too large frictional resistance component in model scale. The effect of the under-prediction of form resistance to the full scale viscous resistance will be discussed in Section 5.4.2.

Form factors with numerical friction lines for KVLCC2 are presented in Fig. 13. Opposing to the results from the ITTC-57 line, the mean value of the form factors with NFL are almost identical for both speeds. Close investigation on the individual simulation points between the different speeds also support this suggestion except the simulations from Strathclyde (Participant 8) and the coarse grids of SSPA/CTU (Participant 6). KVLCC2 in both loading conditions shows smaller speed dependency with ITTC-57 line compared to KCS as the Reynolds number difference between the two speeds is smaller. It is worth noticing that the speed dependency is larger in design condition than the ballast loading condition with the ITTC-57 line. This is a consequence of the “artificial” steepness of the ITTC-57 line which increases as the  $Re$  decreases. Therefore, as any other model with big scale factor (the ratio of ship to model length) would, KVLCC2 model in design condition suffers more from the scale effects with the ITTC-57 line.

The standard deviations of the form factor in percentage of  $(1 + \bar{k})$  predictions for all cases are presented in Table 9. Using the Katsui line, the standard deviation of the form factor are the same in all cases compared to using the ITTC-57 line as the same computations were used. Form factors with NFL showed an increase in the standard deviation for the KVLCC2 in design condition. However, the standard deviation is reduced significantly for KVLCC2 in ballast loading condition and especially for KCS due to a decrease in variation of form factors obtained from different turbulence models. Even though the dependence of turbulence models on form factor seems to decrease by the adoption the NFL of the same code and turbulence model as the double body simulation, the form factors are not expected to be the same for different turbulence models. Application of NFL for different turbulence models arranges the quantity of form resistance with respect to the friction line of the respective turbulence model. As a result, nearly the same full scale viscous resistance values can be obtained by the different turbulence models as shown in Section 5.4.2.

As an alternative to the CFD based form factor determination method used in this study, Wang et al. (2016) and Terziev et al. (2019) calculated the form factors simply by dividing the viscous pressure coefficient to friction coefficient ( $k = C_{PV}/C_F$ ) obtained from the double body simulation with the hull. Therefore, the need of any friction line is removed for form factor determination. This method of form factor determination is dismissed in this study because of the deviation from

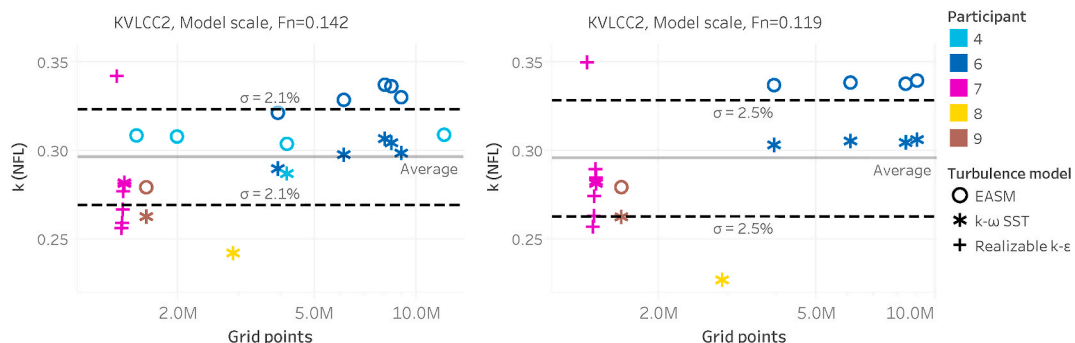


**Fig. 13.** Form factor,  $k$ , based on numerical friction lines versus grid size for KVLCC2 hull in design loading condition at  $Fn = 0.142$  (left) and  $Fn = 0.119$  (right).



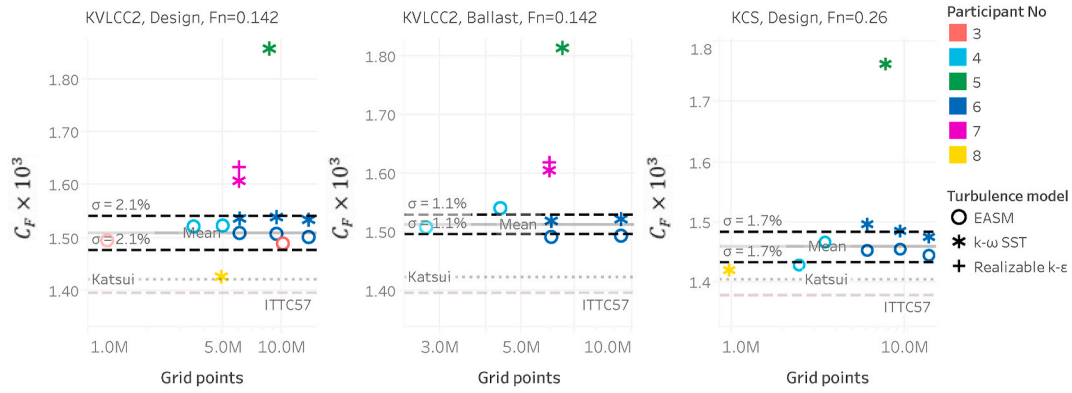


**Fig. 14.** Full scale CFD simulations. Computed frictional coefficient,  $C_F$ , for KVLCC2 hull in design loading condition at  $Fn = 0.142$  (left), KVLCC2 in ballast loading condition  $Fn = 0.142$  (center) and KCS hull in design loading condition at  $Fn = 0.26$  (right).

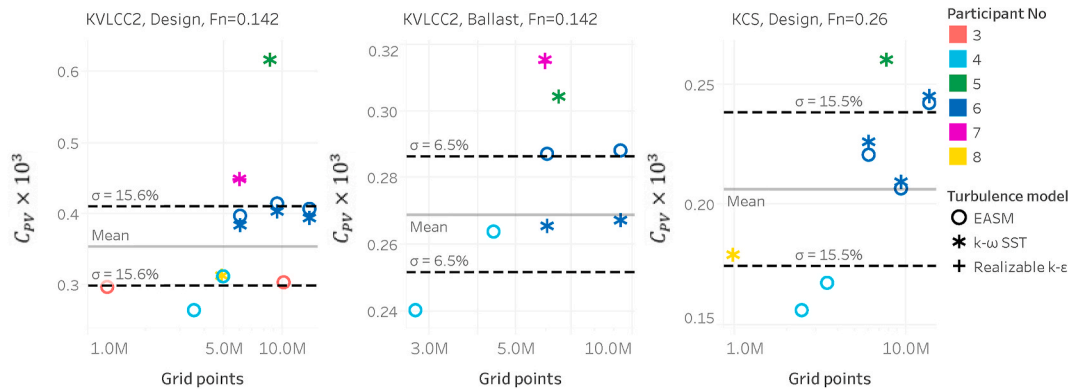


**Fig. 15.** Full scale CFD simulations. Computed viscous pressure coefficient,  $C_PV$ , for KVLCC2 hull in design loading condition at  $Fn = 0.142$  (left), KVLCC2 in ballast loading condition  $Fn = 0.142$  (center) and KCS hull in design loading condition at  $Fn = 0.26$  (right).

the approach of Hughes (1954) as  $C_F$  from double body computation already includes the additional skin friction caused by the curvature effects which should have been included the form resistance as explained in Section 2.

#### 5.4. Full scale predictions

##### 5.4.1. Statics of computed $C_F$ and $C_{PV}$ in full scale

Full scale double body simulations are performed according to the conditions described in Table 2. The friction and viscous pressure

resistance coefficients are presented in Fig. 14 and Fig. 15, respectively. The mean and standard deviation of the computed resistance coefficients are calculated excluding the results from NRC-OCRE and SSSRI who encountered difficulties with grid generation. The mean of  $C_F$  is by approximately 6% and 3% higher than the Katsui line due to additional skin friction caused by the curvature effects for KVLCC2 and KCS, respectively. The standard deviation of  $C_F$  in full scale is reduced considerably compared to model scale for KVLCC2 at both loading conditions mainly because of the reduction of dependence on turbulence models. The standard deviation of  $C_F$  is similar both in model and full

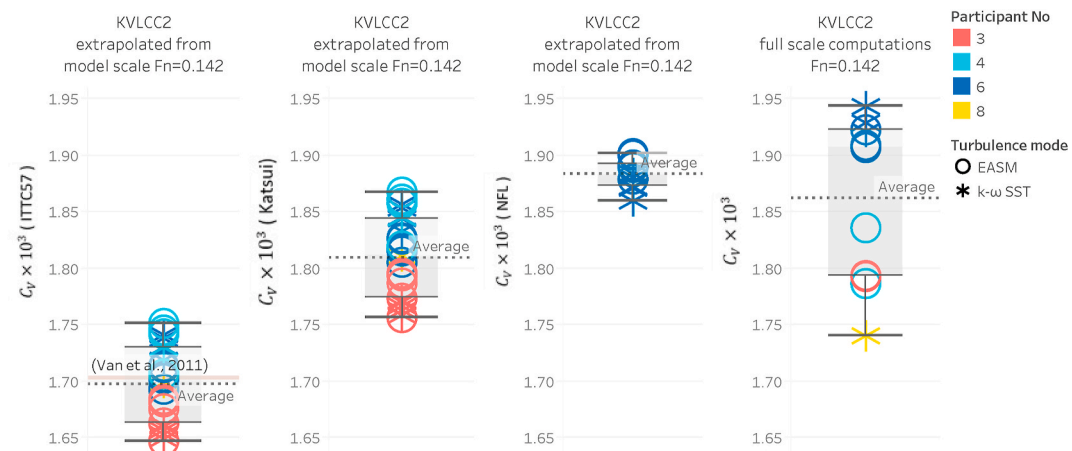


**Fig. 16.** Extrapolated and directly computed full scale viscous resistance coefficients,  $C_V$ , for KVLCC2 hull in design loading condition at  $Fn = 0.142$ .



scale for the KCS hull. However, the standard deviation of  $C_{PV}$  is increased for KCS and KVLCC2 in design condition compared to model scale while the variation of  $C_{PV}$  is similar in model and full scale for KVLCC2 in ballast condition. Considering the standard deviation and the quantity of  $C_F$  and  $C_{PV}$  observed in full scale simulations, the viscous pressure resistance component is the dominant source of variation in  $C_V$ .

As mentioned earlier, the difficulties in the grid generation for NRC-OCRE and SSSRI can be observed through the average  $y^+$  values varied between 450 and 750 for NRC-OCRE and 8300 to 15,000 for SSSRI. As a result, mainly the predicted  $C_F$  values are significantly higher than the mean of the rest of the computations. A strong dependence on turbulence model was observed with the computations of SSPA/CTU in model scale. However, this dependence is reduced by half for SSPA/CTU except the KVLCC2 in ballast loading condition. NMRI performed two simulations per case where one with wall resolved (higher number of grid cells) and the other with wall function where the latter under-predicted both friction and viscous pressure resistance coefficients compared to wall resolved approach.

#### 5.4.2. Full scale viscous resistance extrapolation

Full scale viscous resistance predictions of KVLCC2 and KCS hulls are performed via extrapolation from model scale and compared with full scale computations in Fig. 16 and Fig. 17. The extrapolation to full scale is performed using the CFD based form factors and the ITTC-57, Katsui and numerical friction lines. In Figs. 16 and 17, full scale viscous resistance predictions are presented as box-and-whisker plots with the markers. The participants without full scale computations are excluded for clarity and fair comparison between extrapolated values and full scale computations. The friction line used for the extrapolation and form factor determination is indicated within brackets on the y-axis label.

The extrapolations based on the model tests data of Van et al. (2011) with the ITTC-57 line is represented by a horizontal line that is almost coinciding with the mean  $C_V$  values of the predictions from CFD based form factors for both KVLCC2 and KCS. When the ITTC-57 line is used, full scale viscous resistance of KVLCC2 and KCS are approximately 6.6% and 5.5% lower on average compared to extrapolation based on Katsui line. The mean of the extrapolations based on the ITTC-57 line is 9.7% and 8.0% lower than the full scale computations for KVLCC2 and KCS, respectively. Similar conclusions were obtained by the investigations performed by Raven et al. (2008) on a containership which showed that  $C_V$  from direct full scale computations are 7.4% higher than the extrapolation method with the ITTC-57 line. This difference is mainly due to too steep the ITTC-57 line which causes an underestimated  $C_V$  at full scale. Raven et al. (2008) suggested that the underestimation of  $C_V$  due to the ITTC-57 line is mainly compensated by the correlation allowance ( $C_a$ ) in the ITTC scaling procedures.

Using the same model scale simulations but form factors and extrapolation with the Katsui line, the full scale viscous resistance values are similar to the predictions of full scale simulations. The  $C_V$  predictions with numerical friction lines are only performed with SSPA/CTU as others did not have numerical friction lines. The mean of extrapolated full scale viscous resistance with NFL are in agreement with the mean of full scale computation results. However, the extrapolated values are slightly under-predicted compared to direct full scale computations for both hulls. Agreement between the extrapolations with the Katsui line and NFL is also noticeable.

As can be seen in Figs. 16 and 17, the standard deviation of full scale computations are twice as large as the standard deviation of model to full scale extrapolations with the ITTC-57 and Katsui lines for both hulls. This means that full scale simulations are still less reliable than the model scale computations as the agreement on the CFD predictions are higher in model scale. The standard deviations of extrapolations with the ITTC-57 and Katsui lines are almost identical. But as discussed in Section 5.3, the speed dependency on the form factor was noticeably reduced with the Katsui line compared to the ITTC-57 line. When numerical friction lines are considered, only the results from the SSPA/CTU are considered for the comparison of the standard deviations for a fair comparison. For KVLCC2 and KCS, the smallest standard deviations are observed with extrapolation with the numerical friction lines which also eliminated the speed dependency of the form factors almost completely.

The extrapolated full scale viscous resistance values presented in Figs. 16 and 17 were based on the model scale computations performed at  $Fn = 0.142$  and  $Fn = 0.26$  for KVLCC2 in design loading condition and KCS, respectively. As presented in Table 9, the form factors were speed dependent when ITTC-57 and Katsui lines were used. Therefore, the extrapolated  $C_V$  values would be approximately 1.2% and 0.7% lower than the  $C_V$  values presented in Figs. 16 and 17 when the model scale computations at  $Fn = 0.119$  and  $Fn = 0.152$  are used with ITTC-57 and Katsui lines, respectively. On the other hand, the application of NFL eliminated the speed dependency of the form factors almost completely as shown in Table 9.

The standard deviation is perhaps a more essential measure for improving the power predictions compared to the absolute values of  $C_V$  predictions. As long as  $C_V$  is predicted with the same tendency, correlation factors ( $C_p$  or  $C_A$ ) based on the experience of each institution can be used effectively to adjust the final predictions in terms of absolute values.

## 6. Conclusions

This paper presents an investigation on CFD based form factor

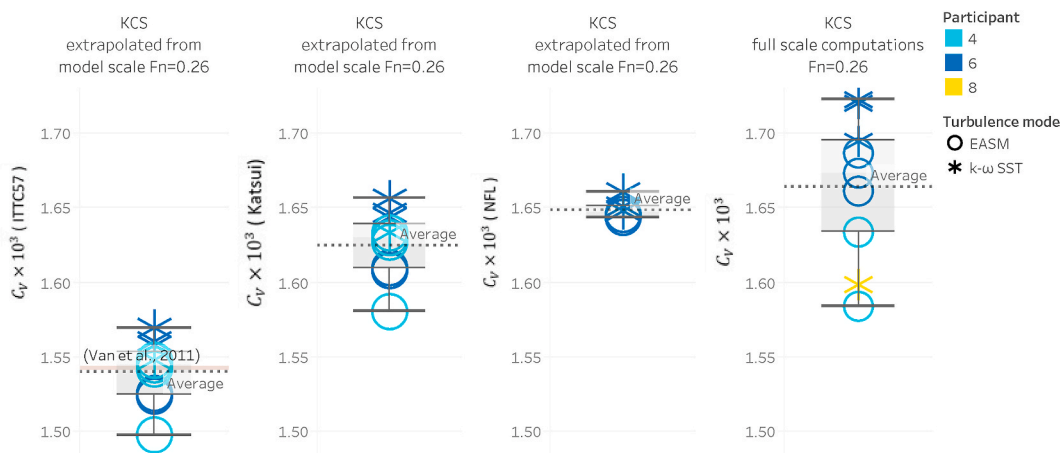


Fig. 17. Extrapolated and directly computed full scale viscous resistance coefficients,  $C_V$ , for KCS hull in design loading condition at  $Fn = 0.26$ .

methods which was initiated by the ITTC Specialist Committee Combined CFD/EFD Methods. The assumptions underlying the form factor approach and the Prohaska method is discussed and model test data is compared to the RANS simulations performed by 7 different CFD codes.

The disposition to leave the Prohaska method of form factor determination is explained through two types of uncertainty.

- The linear relationship proposed by Prohaska in Eq. (5) is not valid for the hulls with prominent bulb designs at fully or partially submerged conditions. Since a substantial portion of the merchant and naval fleet are equipped with bulbous bows, the validity of the Prohaska method as a common tool for all hull forms is under question. As discussed in Section 2, it is difficult to quantify this uncertainty as the case sensitivity is very high.
- The second uncertainty source of the Prohaska method originates from the experimental uncertainty. As demonstrated with the model tests results of KVLCC2 in ballast condition, the experimental uncertainty is noticeably amplified for the form factor as a result of the regression analysis. This amplification of the uncertainty on the form factor can be much more severe if a hull with voluminous bulb is tested where the  $C_T/C_F$  values often cannot be used in low speed range. Therefore, uncertainty of 0.022 (within 95% confidence interval) on the form factor with Prohaska method on KVLCC2 in ballast condition can be considered merely as a best case scenario.

Model scale simulations are performed with seven different codes and six different turbulence models with wall functions and wall resolved approaches. The resulting form factor predictions with the ITTC-57 line from the computations with recommended or standard CFD setups compared well with the experimentally determined form factors for KVLCC2 and KCS in design loading condition at design speeds. The CFD based form factors are mostly under-predicted for KVLCC2 in ballast loading condition compared to experiments. However, the majority of the CFD based form factors were within the experimental uncertainty. The form factors showed 1.5–2.5% standard deviation in percentage of  $(1 + \bar{k})$  even though the abundance of unsystematically varied methods and grids. It should be noted that the experimental uncertainty of the form factor will be of similar levels even for the cases when the linear relationship proposed by Prohaska holds.

Model scale computations include not only the CFD setups according to the best practice guidelines or standard settings but also setups that deviated from the recommended guidelines as one of the goal of this study is to identify the methods that are not well suited for the form factor determination. The resulting form factor predictions with the ITTC-57 line from the computations with non-standard CFD setups.

- indicated that describing the boundary layer with a good quality grid in terms of the grid resolution and the first cell size normal to the wall is essential for both wall treatment types;
- are considerably more sensitive to the grid density in aftbody than forebody and
- can be sensitive to the different types of wall functions with certain turbulence models such as realizable  $k - \epsilon$ .

As mentioned before, different codes indicated varying dependencies on CFD setups, and therefore general recommendations for all CFD setups cannot be made specifically for the sake of form factor determination. Instead, it is observed that most of the codes with a certain CFD setup showed consistent patterns of form factor predictions among different test cases. If these trends are confirmed with more hulls and test cases, application of correlation factors ( $C_p$  or  $C_A$ ) unique for each code and method will be able to reduce the differences in full scale predictions further.

Speed dependency of the form factors are confirmed with the application of the ITTC-57 line for all test cases. The question of which

model scale speed should be chosen for the CFD based form factors with the ITTC-57 line cannot be answered within the scope of this study because of the differing trends of each code. However, the mean values of form factors with ITTC-57 line are closer to the experimental values in design speeds of KVLCC2 and KCS hulls. If another friction line is preferred such as the Katsui or numerical friction lines, the speed dependency on the form factor is reduced significantly, and therefore decreasing the importance of the choice of the speed for the model scale simulations.

Full scale viscous resistance is calculated by extrapolating the model-scale results with different friction/correlation lines and direct full scale simulations. The scatter among the full scale computations are substantially higher than the extrapolations from the model scale for both KVLCC2 and KCS hulls. Even though the standard deviation of  $C_F$  in full scale computations is reduced considerably compared to model scale computations for KVLCC2 at both loading conditions as a result of reduced dependence on turbulence models, the increased discrepancy on full scale  $C_{PV}$  predictions lead to a larger scatter of  $C_V$  for full scale simulations. Hence, the full scale simulations should not to be preferred over the form factor approach yet.

Finally, CFD based form factors can be considered as an alternative or supplementary method to the Prohaska method. It is considered as a step towards answering the request of ITTC Performance Committee of 1978: "Future developments for the determination of form factors on a more scientific basis is expected" (ITTC, 1978). The selection of friction lines would also have an impact on reducing the scatter between the full scale predictions and sea trials due to elimination of scale effects. However, the improvements expected from a change of friction line are minor compared to the implementation of a CFD based form factor method.

Although there are still shortcomings with full scale resistance predictions, combination of EFD and CFD is expected to provide immediate improvements to the 1978 ITTC Performance Prediction Method. Further studies should be performed with many more test cases and CFD codes to establish a better understanding for the dependencies of CFD methods on the form factor prediction. As a final step, comparison of sea trials and the power predictions with CFD based form factors should be performed for different types of ships.

#### CRediT authorship contribution statement

**Kadir Burak Korkmaz:** Conceptualization, Methodology, Validation, Formal analysis, Investigation, Data curation, Writing - original draft, preparation, Writing - review & editing, Visualization. **Sofia Werner:** Conceptualization, Methodology, Investigation, Writing - review & editing, Supervision, Project administration, Funding acquisition. **Nobuaki Sakamoto:** Investigation, Writing - review & editing. **Patrick Queutey:** Investigation, Writing - review & editing. **Ganbo Deng:** Investigation, Writing - review & editing. **Gao Yuling:** Investigation, Writing - review & editing. **Dong Guoxiang:** Investigation, Writing - review & editing. **Kevin Maki:** Investigation, Writing - review & editing. **Haixuan Ye:** Investigation, Writing - review & editing. **Ayhan Akinturk:** Investigation, Writing - review & editing. **Tanvir Sayeed:** Investigation, Writing - review & editing. **Takanori Hino:** Investigation, Writing - review & editing. **Feng Zhao:** Investigation, Writing - review & editing. **Tahsin Tezdogan:** Writing - review & editing. **Yigit Kemal Demirel:** Investigation, Writing - review & editing. **Rickard Bensow:** Conceptualization, Methodology, Investigation, Writing - review & editing, Supervision.

#### Declaration of competing interest

The authors declare that they have no known competing financial interests or personal relationships that could have appeared to influence the work reported in this paper.

## Acknowledgments

The contribution by SSPA/CTU was funded by VINNOVA, the Swedish Governmental Agency for Innovation Systems, grant 2017-02953, and the computational resources provided by Chalmers Center for Computational Science and Engineering (C3SE).

The contribution by NMRI was partially funded by JSPS Grant-in-Aid for Scientific Research (C) #19k04872.

The contribution by ECN/CNRS was granted access to the HPC resources of CINES and IDRIS computing centres under the allocations 2019-A0052A01308 and 2020-A0072A01308 made by GENCI (Grand Équipement National de Calcul Intensif).

The contribution by UM was supported by the US Office of Naval Research and the computational resources and services provided by Advanced Research Computing at the University of Michigan, Ann Arbor.

The contribution by YNU was supported by JSPS (Japan Society for the Promotion of Science) KAKENHI grant number JP18H01638.

## References

- Dogrul, A., Song, S., Demirel, Y.K., 2020. Scale effect on ship resistance components and form factor. *Ocean. Eng.* 209, 107428. <https://doi.org/10.1016/j.oceaneng.2020.107428>. <http://www.sciencedirect.com/science/article/pii/S0029801820304534>.
- Eça, L., Hoekstra, M., 2008. The numerical friction line. *Journal of Marine Science and Technology*. *Journal of Marine Science and Technology* 13, 328–345. <https://doi.org/10.1007/s00773-008-0018-1>.
- Eça, L., Hoekstra, M., 2014. A procedure for the estimation of the numerical uncertainty of cfd calculations based on grid refinement studies. *J. Comput. Phys.* 262, 104–130. <https://doi.org/10.1016/j.jcp.2014.01.006>.
- García Gómez, A., 2000. On the form factor scale effect. *Ocean. Eng.* 26, 97–109.
- Hughes, G., 1954. Friction and form resistance in turbulent flow, and a proposed formulation for use in model and ship correlation. *R. I. N. A.* 96.
- IMO, 2011. Annex 19: Resolution MEPC, vol. 203, 62.
- ITTC, 1957. Subjects 2 and 4 Skin Friction and Turbulence Stimulation.
- ITTC, 1972. Report of Performance Committee.
- ITTC, 1975. Report of Performance Committee.
- ITTC, 1978. Report of Performance Committee.
- ITTC, 2014a. 1978 ittc performance prediction method. ITTC – Recommended Procedures and Guidelines 7, 5-02-03-01.4.
- ITTC, 2014b. General guideline for uncertainty analysis in resistance tests. ITTC – Recommended Procedures and Guidelines 7, 5-02-02-02.
- ITTC, 2014c. Ship models. ITTC – Recommended Procedures and Guidelines 7, 5-01-01-01.
- ITTC, 2017. Uncertainty analysis in cfd verification and validation, methodology and procedures. ITTC - Quality System Manual Recommended Procedures and Guidelines 7, 5-03-01-01.
- Katsui, T., Asai, H., Himeno, Y., Tahara, Y., 2005. The proposal of a new friction line. In: Fifth Osaka Colloquium on Advanced CFD Applications to Ship Flow and Hull Form Design, Osaka, Japan.
- Korkmaz, K.B., Werner, S., Bensow, R., 2019a. Investigations for cfd based form factor methods. In: Numerical Towing Tank Symposium (NuTTS 2019).
- Korkmaz, K.B., Werner, S., Bensow, R., 2019b. Numerical friction lines for cfd based form factor determination method. In: VIII International Conference on Computational Methods in Marine Engineering MARINE 2019.
- Larsson, L., Stern, F., Visonneau, M., 2014. Numerical Ship Hydrodynamics: an Assessment of the Gothenburg 2010 Workshop. Springer. <https://doi.org/10.1007/978-94-007-7189-5>.
- Lindgren, H., Dyne, G., 1980. Ship Performance Prediction. SSPA Publication No. p. 85.
- Niklas, K., Prusko, H., 2019. Full-Scale CFD Simulations for the Determination of Ship Resistance as a Rational, Alternative Method to Towing Tank Experiments. *Ocean Engineering* 190. <https://doi.org/10.1016/j.oceaneng.2019.10643>.
- Pereira, F.S., Eça, L., Vaz, G., 2017. Verification and validation exercises for the flow around the KVLCC2 tanker at model and full-scale Reynolds numbers. *Ocean. Eng.* 129, 133–148. <https://doi.org/10.1016/j.oceaneng.2016.11.005>.
- Ponkratov, D., 2016. 2016 workshop on ship scale hydrodynamic computer simulation. In: Ponkratov, D. (Ed.), Ioyd's Register Workshop on Ship Scale Hydrodynamics. <https://doi.org/10.1016/j.oceaneng.2019.10643>.
- Prohaska, C.W., 1966. A Simple Method for the Evaluation of the Form Factor and Low Speed Wave Resistance. *Proceeding of 11th ITTC*.
- Raven, H.C., van der Ploeg, A., Starke, A.R., Eça, L., 2008. Towards a cfd-based prediction of ship performance - progress in predicting full-scale resistance and scale effects. *International Journal of Maritime Engineering Transactions of the Royal Institution of Naval Architects Part A*.
- SIMMAN, 2008. Simman 2008 Workshop Verification and Validation of Ship Manoeuvring Simulation Methods. [http://www.simman2008.dk/KVLCC/KVLCC2/kvlcc2\\_geometry.html](http://www.simman2008.dk/KVLCC/KVLCC2/kvlcc2_geometry.html).
- Sun, W., Qiong, H., Jia, S., Jie, X., Jinfang, W., Guofu, H., 2020. Numerical analysis of full-scale ship self-propulsion performance with direct comparison to statistical sea trial results. *J. Mar. Sci. Eng.* 8 <https://doi.org/10.3390/jmse8010024>. <https://www.mdpi.com/2077-1312/8/1/24>.
- Terziev, M., Tezdogan, T., Incecik, A., 2019. A geosim analysis of ship resistance decomposition and scale effects with the aid of CFD. *Appl. Ocean Res.* 92 <https://doi.org/10.1016/j.apor.2019.101930>.
- Toki, N., 2008. Investigation on correlation lines through the analyses of geosim model test results. *J. Jpn. Soc. Nav. Archit. Ocean Eng.* 8, 71–79.
- Tokyo, 2015. Tokyo 2015 a Workshop on Cfd in Ship Hydrodynamics. <https://t2015.nmri.go.jp/kcs.html>.
- Van, S.H., Ahn, H., Lee, Y.Y., Kim, C., Hwang, S., Kim, J., Kim, K.S., Park, I.R., 2011. Resistance characteristics and form factor evaluation for geosim models of KVLCC2and KCS. In: Advanced Model Measurement Technology for EU Maritime Industry.
- Wang, J., Yu, H., Zhang, Y., Xiong, X., 2016. CFD-based method of determining form factor k for different ship types and different drafts. *J. Mar. Sci. Appl.* 15, 236–241.
- Wang, J.B., Yu, H., Feng, Y., 2019. Feasible study on full-scale delivered power prediction using CFD/EPD combination method. *J. Hydrodyn.* 31 <https://doi.org/10.1007/s42241-019-0075-4>.
- Wang, Z.Z., Xiong, Y., Shi, L.P., Liu, Z.H., 2015. A numerical flat plate friction line and its application. *J. Hydrodyn.* 23, 383–393.
- Xing, T., Stern, F., 2009. Factors of safety for richardson extrapolation. *Journal of Fluids Engineering-transactions of The Asme - J FLUID ENG* 132, 65. <https://doi.org/10.1115/1.4001771>.
- York, D., Evensen, N., Ló, M., Nez, M., De, J., Delgado, B., 2004. Unified equations for the slope, intercept, and standard errors of the best straight line. *American Journal of Physics - AMER J PHYS* 72. <https://doi.org/10.1119/1.1632486>.